1987

Transition Correlation Studies In A Water Vapour Laser

Paul Adrien Rochefort

CANADIAN THESES

THÈSES CANADIENNES

NOTICE

The quality of this microfiche is heavily dependent upon the quality of the original thesis submitted for microfilming. Every effort has been made to ensure the highest quality of reproduction possible.

If pages are missing, contact the university which granted the degree.

Some pages may have indistinct print especially if the original pages were typed with a poor typewriter ribbon or if the university sent us an inferior photocopy.

Previously copyrighted materials (journal articles, published tests, etc.) are not filmed.

Reproduction in full or in part of this film is governed by the Canadian Copyright Act, R.S.C. 1970, c. C-30.

AVIS

La qualité de cette microfiche dépend grandement de la qualité de la thèse soumise au microfilmage. Nous avons tout fait pour assurer une qualité supérieure de reproduction.

S'il manque des pages, veuillez communiquer avec l'université qui a conféré le grade.

La qualité d'impression de certaines pages peut laisser à désirer, surtout si les pages originales ont été dactylographiées à l'aide d'un ruban usé ou si l'université nous a fait parvenir une photocopie de qualité inférieure.

Les documents qui font déjà l'objet d'un droit d'auteur (articles de revue, examens publiés, etc.) ne sont pas microfilmés.

La reproduction, même partielle, de ce microfilm est soumise à la Loi canadienne sur le droit d'auteur, SRC 1970, c. C-30.

THIS DISSERTATION HAS BEEN MICROFILMED EXACTLY AS RECEIVED

LA THÈSE A ÉTÉ MICROFILMÉE TELLE QUE NOUS L'AVONS REÇUE

TRANSITION CORRELATION STUDIES IN A WATER VAPOUR LASER

by

Paul Adrien Rochefort

Department of Physics

Submitted in partial fulfillment
of the requirements for the degree of
Doctor of Philosophy

Faculty of Graduate Studies
The University of Western Ontario
London, Ontario
July, 1987

ISBN 0-315-36611-7

ABSTRACT

The interaction between several pairs of coupled water vapour lines was investigated with a compound mirror-grating-grating (MGG) laser. The MGG laser allows the simultaneous and co-axial lasing of two wavelengths with the two lines linearly polarized parallel or perpendicular to each other.

The interaction experiments was done with four pairs of competitive water vapour lines; the 26.6 and 47.70, 26.6 and 47.47, 27.97 and 47.70, and 27.97 and 47.47 micrometer lines. The coupled lines share an upper or lower energy level so that the power of one or the other or both lines were suppressed when they lased simultaneously.

From interaction results of 26.6 and 47.70 micrometer lines, the parallel polarized line coupling constant was 0.18 ± 0.04, and the perpendicular constant was 0.54 ± 0.06. The ratio of the two coupling constants, which is a ratio of the competition between the two lines for magnetic sub-level population of the shared level, was equal to 0.40 ± 0.14 which compares well with the theoretical value of 0.35.

Although the experimental results of the three other pairs of lines did not allow coupling constants too be calculated because the power change of the short wavelengths was to small to measure with the experimental noise, the power of longer wavelengths were suppressed, demonstrating that the lines was coupled. For two of the pairs, the coupling depended on the relative polarization of the lines: the 47.70 micrometer line was completely suppressed whenever the 27.97 micrometer line lased. The relative suppression with respect to polarization of the 47.70 micrometer line by the 26.6 micrometer line was consistent with the expected results from the given assignment of energy levels, while the suppression of the 47.70 micrometer line by the 27.97 micrometer line was opposite to what was expected.

The single line two perpendicular polarization mode control features of a compound mirror-grating-mirror (MGM) laser were also investigated: the output can be in one or the other or both modes. The resonator's polarization properties are due in part to the different effective phase change upon reflection from the resonator's grating for radiation parallel and perpendicular to the grating lines. This can be expressed as a difference in the effective optical plane positions for the two polarizations. From the simultaneous measurement of the modes with the displacement of the resonator mirrors, the optical plane difference was measured

to be 17 ± 1 micrometers for the 30 micrometer blazed grating used. The ratio of the optical plane difference to the groove depth of the grating was 0.32 ± 0.02, in fair agreement with the theoretical calculated value of 0.21.

ACKNOWLEDGEMENTS

I would like to thank Dr. E. Brannen for his guidance and support during this project, and also to Dr. Z. Kucerovsky for his helpful and pointed suggestions during the project and writing of the thesis.

I would also like to thank Dr. P. Alford, former Head of the Physics Department, and Dr. G. Rose, Chairman of the Physics Department, for making available the facilities of the Department. I am also indebted to all of the support and technical staff of the department for all their help in many varied ways.

Finally, I would like to thank , with all my love, my wife, Francine, for her love, support and many encouragements.

TABLE OF CONTENTS

LIST OF FIGURES

LIST OF TABLES

NOMENCLATURE

c	Speed of light
C	Coupling coefficient
C'	Magnetic coupling coefficient
d	Grating line spacing
E	Electric field strength
E_i	Electric field strength of resenator mode i
f	Mode frequency
Δf	Mode frequency difference
G_1	Primary grating of compound grating resonator
G_2	Secondary grating of a mirror-grating-grating resonator
h	Grating groove depth
I	Laser line intensity
I_1	Coupled line intensity of first laser line
I_2	Coupled line intensity of second laser line
$I_{\frac{1}{1}}$	Single line intensity of first laser line
$I_{\frac{1}{2}}$	Single line intensity of second laser line
J	Quantum angular momentum value
ΔJ	Change in J value for a transition
L	Optical length of a laser resonator
ΔL	Optical length difference of a laser resonator
K_i	Wavenumber of resonator mode i
m	Quantum magnetic sub-level value
Δm	Change in m value for a transition
MG	Mirror-grating laser resonator
MGG	Mirror-grating-grating compound grating laser resonator

MGM	Mirror-grating-mirror compound grating laser resonator
M_1	Principal mirror of a compound grating resonator
M_2	Secondary mirror of a mirror-grating-mirror resonator
n	Diffraction order of a grating
Q	Quality factor of a resonator
$T_{o,\pm}$	Quantum operators for dipole transitions
P	Polarization of the laser medium
P_i	Polarization of the laser medium due to the resonator mode i
α	Net laser gain
β	Saturation parameter of laser line
δ	Optical plane difference coefficient
ϵ_o	Permittivity of free space
θ_B	Blaze angle of a grating
θ_{12}	Cross saturation coefficient of line 2 to line 1
λ	Radiation wavelength
γ_i	Decay constant of energy level i
δ_c	Critical wavelength for total reflection from a grating
λ_i	Pumping rate of level i
π	$\Delta m = 0$ type of transition
ρ_i	Mode pushing term
ρ_{ij}	Density matrix element ij
σ_i	Linear mode pulling term
$\sigma_\pm$	$\Delta m = \pm 1$ type of transition
τ_{12}	Cross pushing term of mode 2 on mode 1
ψ_i	Laser radiation of resonator mode i
φ	Angle of refraction of radiation from a grating

Φ_i Phase of resonator mode i

Ψ Incident angle of radiation on a grating

Ω_i Frequency of resonator mode i

γ_{ij} Dipole moment of transition ij

CHAPTER 1

INTRODUCTION

This thesis is concerned chiefly with the investigation of coupled transitions in the water vapour laser in the far infrared region. Specifically, the coupled transitions studied share an upper or lower energy level, and thus they are in competition for laser gain. The ultimate purpose is the measurement of coupling parameters of pairs of lines, the effect of the relative polarization of the two lines upon the coupling, and the testing of energy level identification.

Since many lasing media can operate on several simultaneous lines and modes, and since for most scientific experiments single line and mode laser operation is usually preferred, numerous optical techniques have been developed to force single line and mode operation of lasers. Among these techniques are the use of a grating or prism in the resonator cavity, dielectric thin film coated mirrors with high narrow-band reflectivity, or intra-cavity Fabry-Perot resonators for mode and frequency discrimination. All of these simple and reliable techniques above have been used with good results. In the far infrared, the lack of low loss

transmission materials restricts severely the optical cavity arrangements possible. For this reason, the use of gratings as mirror and output coupling elements is preferred.

In order to carry out this program, a special type of laser resonator was needed. A compound double grating cavity laser was devised which allowed the selection of specific pairs of lines to undergo simultaneous or alternate lasing with control on the relative polarizations.

The operation of a modified compound grating resonator in single line lasing was first studied. The modified resonator allowed control on two perpendicular polarization resonator modes operating on the same transition. Experiments were carried out to investigate the interaction of the two perpendicular polarized resonator modes with the lasing medium. A grating diffraction model for different radiation polarizations was used to explain the interaction between the two perpendicular modes. A significant characteristic of the grating is the difference in effective phase change upon reflection and diffraction of the incident radiation for the two polarizations parallel or perpendicular to the grating lines. This characteristic is important in the operation of the compound grating resonator.

The coupling of several pairs of water vapour laser lines was then studied with the compound grating laser. These

coupled lines were in competition for laser gain. Coupling constants were calculated from the fractional change in the lasing power of a pair of lines when operating simultaneously as compared to operating separately. The interrelation of the coupling with the relative polarization of the two lines was also studied and analyzed. Since the theoretical coupling coefficients depend on the characteristics of the energy levels involved, the experimental coupling values test the energy level identifications.

Water vapour was chosen for the coupled transition studies because it has over a hundred pulsed laser lines spanning the range from 7 to 220 micrometers under electric discharge excitation. Many of these lines share a common energy level either in competition or cascade (Benedict et al., 1969) so that water vapour is an excellent medium for this type of study.

CHAPTER 2

THEORY OF COUPLED OPTICAL RESONATORS

Water vapour, like many other laser media, has many lines that can lase simultaneously with an ordinary two mirror optical resonator. One method of forcing the laser to operate on a single line is the use of a grating as one of the end mirrors. In this chapter, the theory of a mirror-grating (MG) laser cavity will be described, as well as the theory two versions of compound grating cavities. The first compound resonator version allows polarization control over the laser radiation, while the second described configuration allows in practice two and only two laser lines to operate simultaneously when the gain of the lines permit.

2.1 MIRROR-GRATING RESONATOR

In a simple mirror-grating (MG) laser resonator (see figure 2.1), the grating is set in the Littrow configuration for the desired wavelength. The resonator grating acts as a frequency selective mirror (Brannen, 1965). To reduce the losses to a minimum, the grating must be chosen so that only the first and zeroth order of diffraction are possible for the design wavelength, and the facet angle of the grating should be equal or nearly so to the Littrow angle.

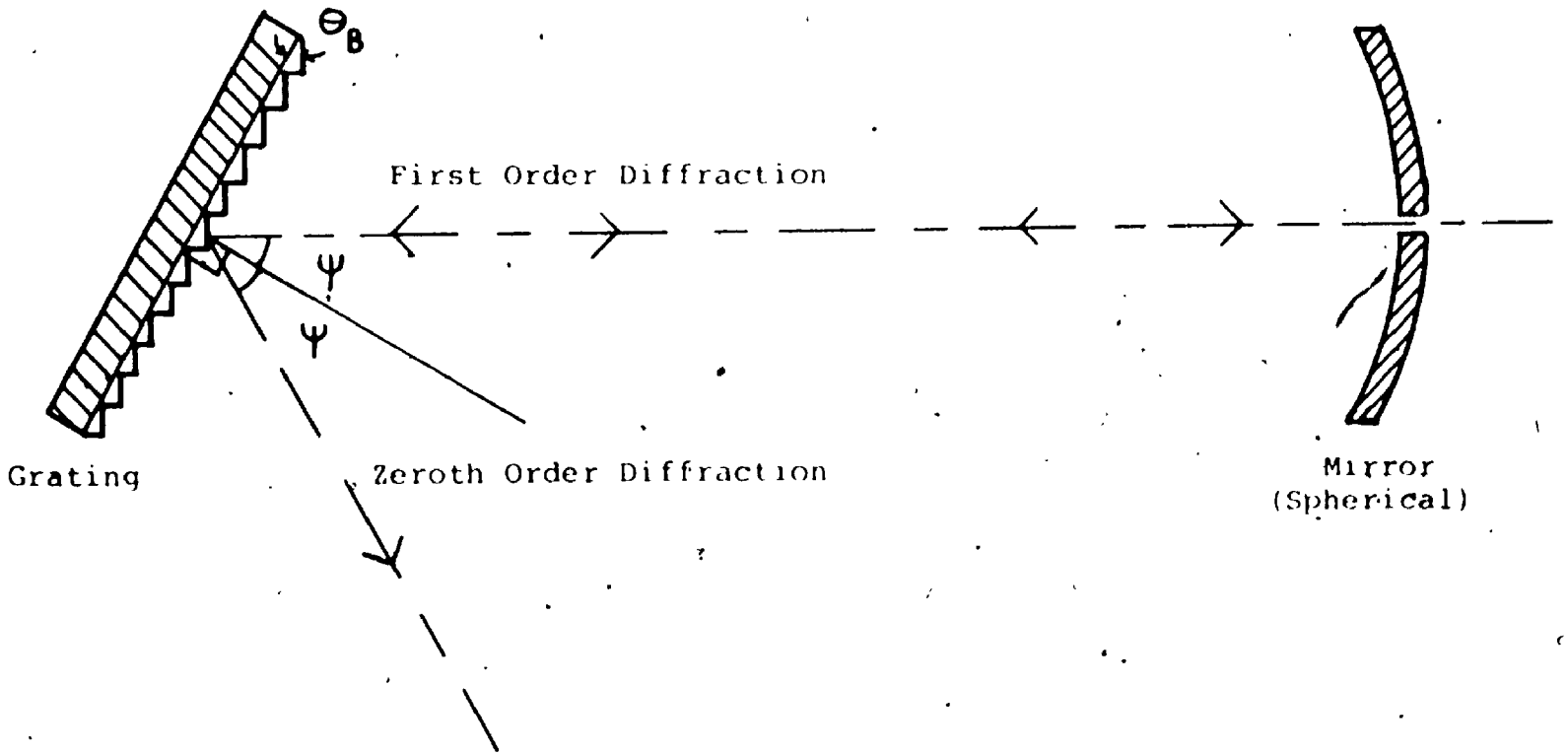

Figure 2-1
Mirror-Grating Laser Resonator

For a specific wavelength, the angle of diffraction from a grating in the Littrow configuration can be calculated from the grating equation

$$n\lambda = d(\sin(\Psi) + \sin(\varphi)) \quad (2.1\text{-}1)$$

where n is the diffraction order, λ is the radiation wavelength, d is the grating line spacing, Ψ is the angle of incidence and φ is the angle of diffraction. Both Ψ and φ are measured from the normal of the grating and are positive on the same side of the normal.

For the first order Littrow configuration,

$$n = 1$$

and

$$\Psi = \varphi$$

so that

$$\lambda = 2d\sin(\Phi)$$

For example, the Littrow angle of incidence for a grating with ruling spacing of 33.33 micrometers for radiation of 27.97 micrometers (a strong water vapour laser line) is 24.83 degrees. The above grating is referred to as a 30 micrometer grating because the Littrow angle for 30 micrometers is equal to the blaze angle of the grating (26.74 degrees).

Because of the grating echelette geometry, laser

radiation from a cavity containing a grating is linearly polarized (Hoeksema et al., 1969, Brannen, 1965). The polarization is caused by the different grating reflection coefficients for radiation parallel and perpendicular to the grating rulings. Specifically, for a grating in the first order Littrow configuration and an angle of incidence of 23.5 degrees, about 98 percent of the radiation polarized perpendicular to the grating lines is diffracted in first order back down the resonator axis with 2 percent in the zeroth order. For parallel polarized radiation approximately 65 percent is diffracted into the first order and 35 percent in the zeroth order (Brannen and Rumbold, 1969). The parallel polarized radiation will not lase because of the large reflection into the zeroth order, and so only the perpendicularly polarized mode lases. Often, the small amount of perpendicular radiation that is diffracted into the zeroth order is used as the laser output.

One effect which must be kept in mind is the lasing of strong lines whose wavelengths are simple integral fractions ($\lambda/2, \lambda/3$ and so forth) of the design wavelength corresponding to higher order of diffraction from the laser grating. In these cases the polarization effects are not as distinct. For example the 27.97 micrometers line lasing in the fourth order of the 118 micrometer grating has almost no prefered polarization.

2.2 COMPOUND RESONATOR

In the diffraction of polarized radiation by a grating the effective phase change upon reflection is different for radiation polarized parallel and perpendicular to the grating grooves. Thus the effective optical plane of the grating is located at different distances from the grating surface for parallel and perpendicular polarization. Because this grating characteristic is important in explaining some of the features of the compound grating resonator, it will be discussed in the first parts of this section. The second and third part describe the two versions of the compound grating resonator used in the laser for the thesis. The final section is a derivation to calculate the optical path difference in the compound resonators arising from optical plane position differences.

2.2.1 OPTICAL PLANE POSITION FOR GRATINGS

The interaction of polarized radiation with a reflection echellete grating is a very difficult theoretical problem even though the scalar diffraction equation is well known. Experimentally, gratings show quite different diffraction intensities depending on the relative polarization of the incident radiation to the grating lines (Petit, 1980).

The phase change of radiation diffracted and reflected by a grating is important in understanding the laser polarization properties using compound grating resonators. From the

basic boundary conditions of radiation interacting with the conducting surface of the grating, the phase change will depend upon the relative polarization of the incident radiation (Petit, 1980).

I.H Hutchinson (1981a, b) has written two of the few publications on the polarization reflection phase difference of gratings, and the properties imparted from this difference to optical properties of grating laser resonators.[1] Hutchinson (1981a) used an echelette grating as a resonator element normal to the optical axis. The laser radiation wavelength was at least twice the ruling spacing, so that only zero order diffraction was possible.

Hutchinson observed a heterodyne signal between two laser modes polarized parallel and perpendicular to the grating lines. He deduced that the optical length of the resonator for the two modes was different, and therefore the optical planes of reflection of the grating for the two modes were separated. The optical plane is defined as the location of a hypothetical plane mirror providing the same reflection

---

[1] An analogous phase change relative to the polarization of the incident radiation can be found in strip gratings. Strip gratings are made up of identical parallel strips of metal equally spaced either free standing or supported by a dielectric material. When strip gratings were used in far infrared laser resonators, similar types of results were found as those above (Whitbourm and Macfarland, 1986, Véron and Whitbourn, 1986). Theoretical calculation of the polarization dependent transmission, reflection and phase change of strip gratings can be done using transmission line and characteristic impedance models (Compton el al., 1983)

path as the grating in the far field. The plane is a way of modelling the reflection polarization phase difference of the grating as an optical path difference. From the frequency of the heterodyne signal and the resonator length, Hutchinson was able to calculate the difference of the optical plane positions. Hutchinson used the frequency difference between polarization modes for the measurement of plasmas densities (Hutchinson, 1982).

He also calculated the grating optical plane difference theoretically (Hutchinson, 1981b), the results being in good agreement with the experimental values. Hutchinson calculated the optical plane difference with respect to the polarization by matching the "Rayleigh" expanded radiation wavefunction just inside and outside the grating boundary. His calculations were normalized to the groove depth of the grating (distance between top and bottom plane of the rulings), and he defined an optical plane difference coefficient, , as the ratio of the optical plane difference to the groove depth. He calculated that the coefficient was equal to about 0.213, and that the the coefficient changed very slowly to a minimum of 0.167 for very long wavelengths with respect to the groove depth. In Hutchinson's calculations, a symmetrical triangular rule profile, blazed at 45 degrees, was assumed. Hutchinson maintained that these results would also hold for gratings blazed not too far of 45 degrees. Experimentally, he found only 20 percent difference between the theoretical value and

the experimental value of the optical plane difference for a grating blazed at 24.5 degrees (Hutchinson, 1981a, b).

For both types of compound grating resonator described in the following sections the reflected radiation is not normal to the grating, and for the first type of resonator the incident wavelength is approximately the same length as the grating line spacing. However, the optical plane model outlined above is useful in explaining characteristics of the resonators. From experimental results with a mirror-grating-mirror resonator a measure of the optical plane difference was calculated (see chapter 5).

2.2.2 MIRROR-GRATING-MIRROR RESONATOR

If a mirror is placed in such a position that the radiation diffracted into the zeroth order from the grating of an MG resonator is reflected back to the grating and hence down the axis of the laser in phase with the first order reflection, the parallel polarization mode will have small enough losses so that it can lase as well (see figure 2.2). This mirror-grating-mirror (MGM) configuration allows the laser action with both polarizations and still maintains frequency selective characteristics (Brannen and Sarjeant, 1970). [2]

---

[2] It will be shown later that the wavelengths longer than a critical value will be completely reflected from the primary grating. The MGM configuration then can act as a resonator for these long wavelengths. This long wavelength lasing can be controlled by an iris placed in the optical

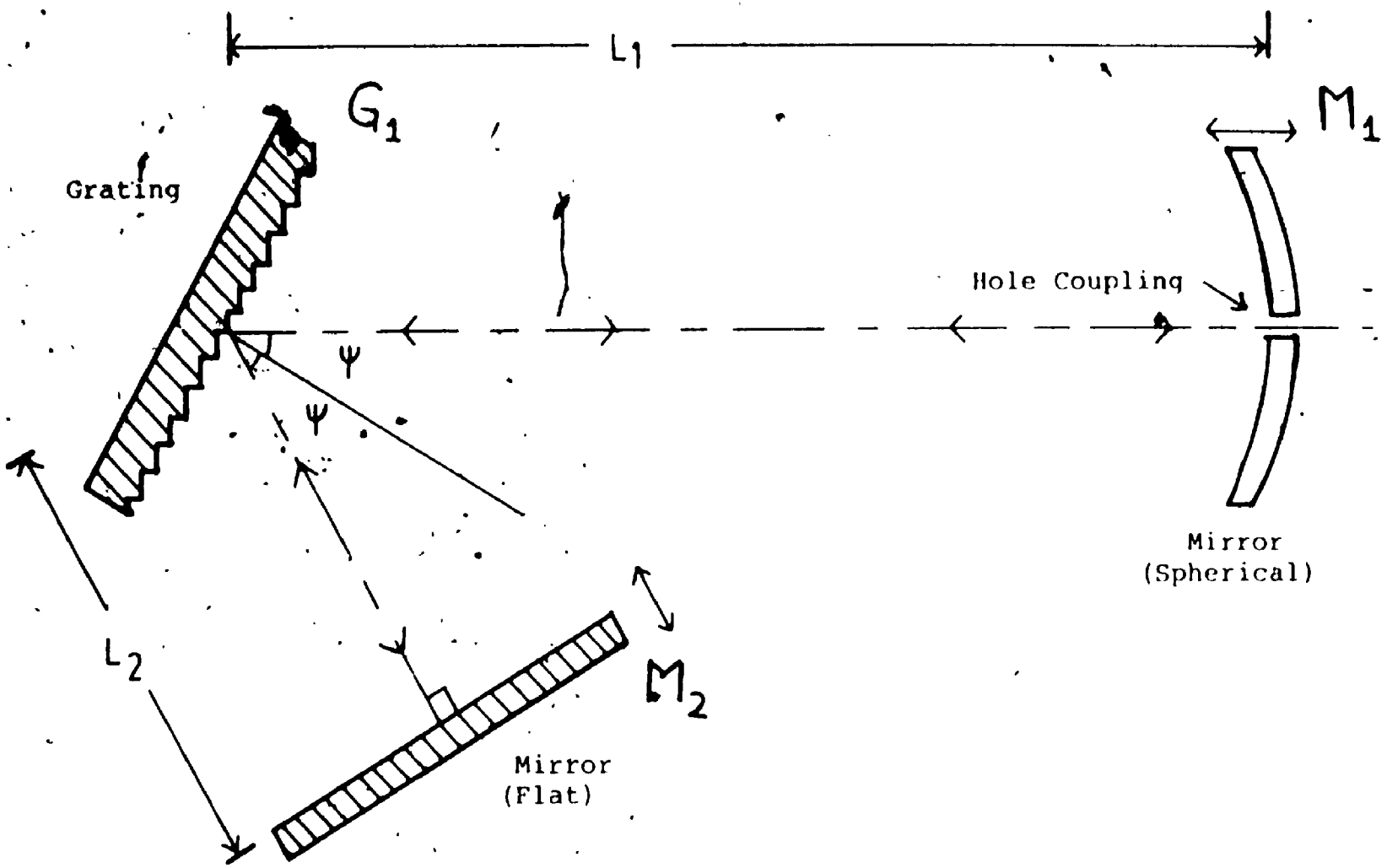

Figure 2-2
Mirror-Grating-Mirror Laser Resonator

For both polarization modes, the additional mirror creates a secondary resonator that couples with the principal resonator. The effect of the coupled resonator is especially important for the parallel polarization because a large fraction of radiation is reflected into the secondary resonator.

Theory shows that the secondary cavity modulates the quality factor, Q, of the primary resonator, the Q depending on the relative phase of the two resonators. The primary resonator Q modulation depth depends principally on the degree of coupling between the two resonators. The modulation also depends on the relative phase of the resonator modes. In the coupled cavity, the effect of the second resonator upon the different resonator modes is illustrated in figure 2.3.

In addition to the frequencies existing in the uncoupled primary resonator, additional frequencies exist in the coupled resonator. They depend on the length ratio of the two cavities. For example, if the length ratio between the two cavities is 1/5, the modulation period will be six modes of the coupled resonator, which corresponds to five resonator modes in the uncoupled long resonator. This 20 percent increase in the number of modes reflects the overall degree

---

cavity so that the losses for long wavelength are too great to support laser action.

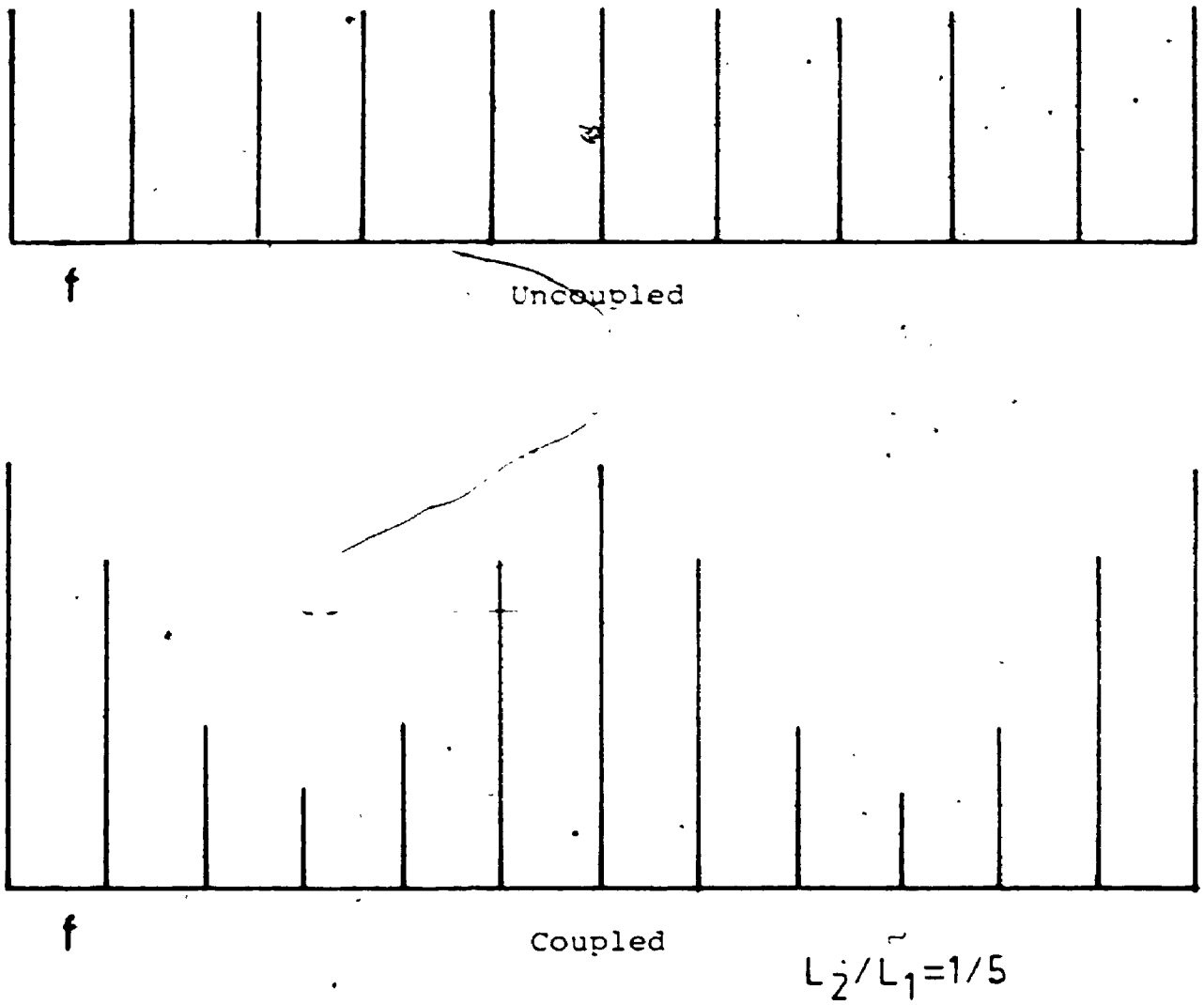

Figure 2-3
Q versus Resonant Mode
of a Coupled and Uncoupled Resonator

of increase in resonator length.

When the uncoupled resonant frequency of the second cavity is equal to the uncoupled resonant frequency of the first cavity, the compound resonator will have the largest Q, and there will be no frequency shift. For modes of one order greater and lower than the unshifted mode (mode where the resonant frequency of the primary and secondary cavity are equal), little frequency shift is noticed between the coupled cavity and the uncoupled primary cavity. (Choo and Brannen, 1971, Kleinman and Kisliuk, 1963).

Because of the optical plane difference of the primary grating, G_1, for the two polarization modes, the coupling effect of the secondary mirror for the two polarizations will not be in phase. In other words the optical length of the secondary cavity is not the same for the two polarization modes because of the optical plane difference of the grating. A more detailed discussion of the above resonator feature and how this relates to the characteristics of the laser can be found in chapter 5 on the experimental results of the MGM laser.

2.2.3 MIRROR-GRATING-GRATING RESONATOR

A compound grating resonator can be made to lase selectively on two laser lines by replacing the secondary mirror of MGM resonator with a grating. In order to have independent

control of the two wavelengths, the wavelength of the second laser line is chosen longer than a critical wavelength $\lambda_c = d(1+\sin(\Psi))$ so that only the zero order diffraction is possible from the primary grating, G_1. The primary grating is as usual in the Littrow configuration for the first wavelength. The primary grating acts as a specular mirror for the second laser line. In order to limit the second line to a specific wavelength, the second grating is set in the Littrow configuration for that wavelength. The second grating, G_2, is also chosen so that only the first and zero orders are possible (see figure 2.4).

For a given incident angle for the primary grating, Ψ_1, the critical wavelength can be calculated from the grating equation.

$$n\lambda = d(\sin(\Psi_1) + \sin(\varphi_1)) \qquad (n=1)$$

Since the incident angle, Ψ_i, is constant then

as λ increases, $\sin(\varphi_1) \rightarrow 1$ or $\varphi_1 \rightarrow 90^\circ$

and the critical wavelength will be

$$\lambda_c = d(1 + \sin(\Psi_1))$$

For example, using as the primary grating the 30 micrometers grating specified before (ruling spacing of 33.33 micrometers, Littrow angle of 24.83 degrees for 27.97 micrometer radiation), the critical wavelength is 47.33 micrometers so that all wavelengths longer than 47.33

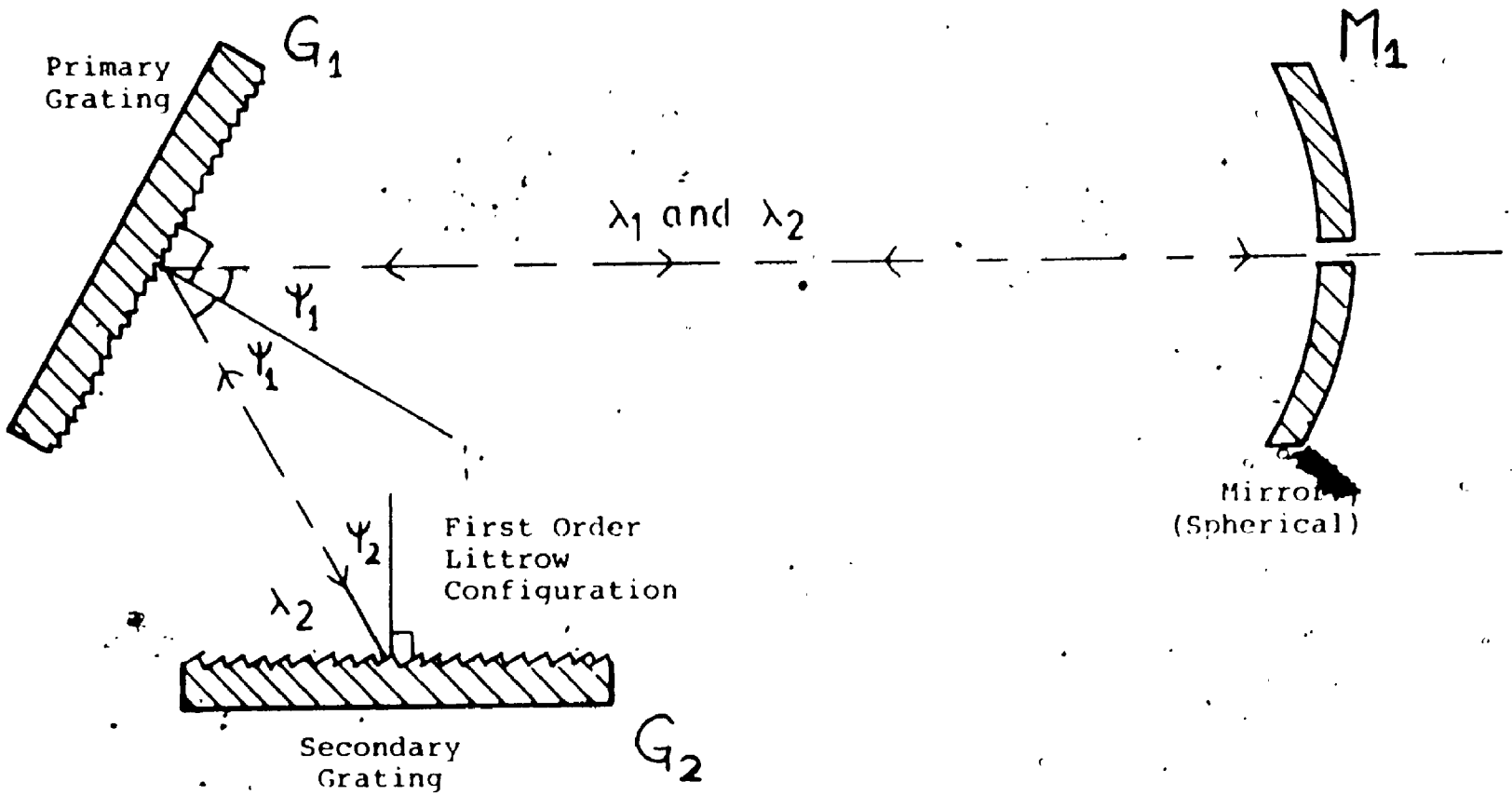

Figure 2-4
Mirror-Grating-Grating Resonator

micrometers are completely reflected in zero order into the secondary cavity.

An important feature of a compound grating resonator is the use of the primary grating as a short wavelength filter for the long wavelength laser line.

For certain lasing media such as water vapour, there is such a large number of laser lines that occasionally a long wavelength line may be close to an integer multiple of a shorter line. If a simple MG resonator is used and if the short wavelength is a strong line, the short wavelength can lase simultaneously with the long one. In such a case, a compound mirror-grating-grating (MGG) resonator can be used to eliminate the short wavelength. The primary grating is chosen and set in such a way that the short wavelength will be diffracted into several orders while the long wavelength will be reflected off the primary grating as if it were a flat mirror.

For example, the 118.6 micrometer line of water vapour is almost an exact multiple of the 39.69 micrometer line, and often, when the laser is aligned with a grating blazed for 118.6 micrometers, the laser will also lase on 39.69 micrometers line, unless the current is restricted. The twin grating compound resonator can eliminate this problem by using a 30

micrometer grating as the primary grating and 118.6 micrometer grating as the secondary grating.

The second laser line existing in the coupled MGG resonator will also be linearly polarized because the second grating is also in the Littrow configuration and it has similar properties as explained before. However, there is one major difference between the polarizations caused by the first and second grating. The polarization of the first laser line is determined by the setting of the primary grating. The relative polarization of the second line is either perpendicular or parallel (or in a special case, both) to the lines of the primary grating depending on the relative angle of second grating lines to the first and was partly controlled by the rotation of the second grating about the optical axis. The polarization features of the second laser line are a function of the difference in the optical plane positions of the primary grating for the two polarizations and thus the difference in optical path length for the two polarization modes. Experimental results demonstrating this polarization feature, and a more elaborate discussion of the optical mechanisms involved can be found in chapter 6.

2.3 OPTICAL PATH DIFFERENCE

As described in the two previous sections, radiation is reflected off the primary grating of the resonator along two different optical paths depending on the polarization of the

radiation. Assuming that the model of a constant or slowly varying optical plane difference is valid, and dependent mainly on the groove depth even when the zeroth order diffraction is reflected off at some angle other than zero (as assumed in Hutchinson's derivation), then the optical path difference for the two polarization modes will simply depend on the reflection angle off the primary grating and the groove depth.

With this model, the optical path difference of the two modes can be easily calculated from the geometry of the laser resonator (figure 2.5). The groove depth (h) can be calculated from the blaze angle (θ_B) and line spacing (d). The grating parameters are specified for each grating.

$$h = d\cos(\theta_B)\sin(\theta_B)$$

Taking into consideration the optical plane difference coefficient (δ) and the incident angle (ψ_i), the optical path difference (ΔL) can be found as

$$\Delta L = 2\delta h\sec(\psi_i)$$

$$\Delta L = 2\delta d\cos(\theta_B)\sin(\theta_B)\sec(\psi_i). \qquad (2.3\text{-}1)$$

It is probable that the optical plane difference coefficient calculated by Hutchinson is not accurate when the reflection angle is far from zero, but hopefully the coefficient is a slowly varying function of the reflection angle and radiation wavelength.

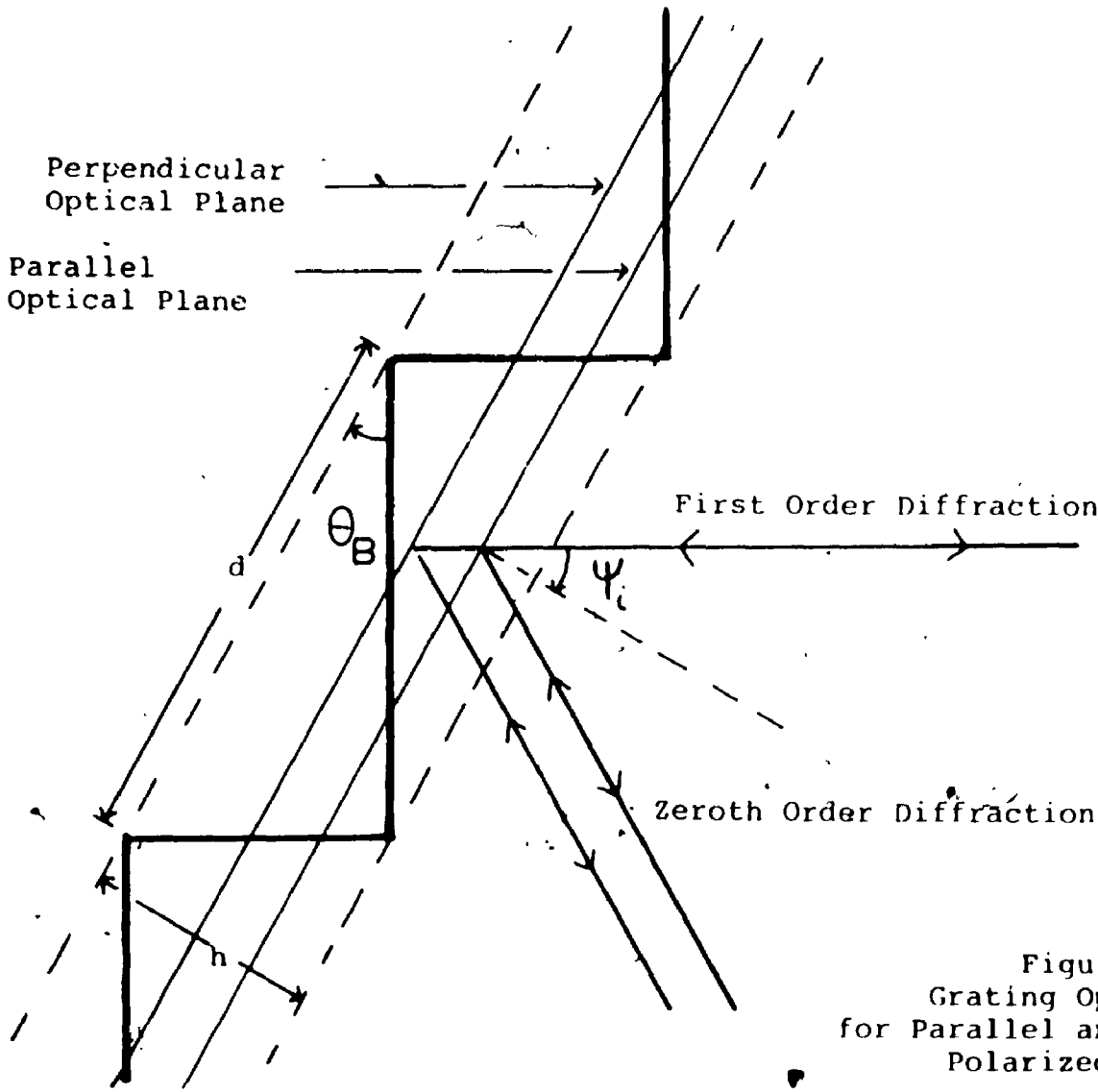

Figure 2-5
Grating Optical Plane
for Parallel and Perpendicular
Polarized Radiation

As an example, the optical path difference can be calculated for the 30 micrometers grating used as the primary grating for many of the experiments done for this thesis. The primary grating has a rule spacing of 33.33 micrometers and a blaze angle of 26.74 degrees. For simplicity, the reflection angle can be assumed to be equal to the blaze angle. Since the optical plane difference coefficient for this type of arrangement is not known, Hutchinson's value of 0.213 can be used for an order of magnitude calculation. The optical path difference is calculated to be 6.39 micrometers.

If the above grating setup was used in an MGM resonator (the iris opened enough to allow the longer wavelength to lase) the optical path difference for the two polarization modes would depend only on the setting of the primary grating, and the two modes would lase at slightly different frequencies. The frequency difference can be calculated from the following derivation.

The ratio of mode frequency difference, Δf, to the resonator frequency is equal to the ratio of the resonator length difference (equal to the grating optical path difference), ΔL, to the resonator length, L,

$$(\Delta f/f) = (\Delta L/L)$$

then the frequency difference is

$$\Delta f = 2\gamma d(c/\lambda)(1/L)\cos(\theta_B)\sin(\theta_B)\sec(\psi_i)$$

Using the grating, wavelength and setting from the previous example and a resonator length of 4.4 meter (the length of the optical cavity used in the experiments for this thesis), the frequency difference would be 9.17 MHz. for the 47.47 micrometers line, and 3.67 MHz. for the 118.6 micrometers line. These frequency differences can be compared to the free spectral range of the laser of 34 MHz and the water vapour Doppler width of 26.1 MHz for 47.47 and 10.5 MHz for 118.6 micrometers line. The Doppler width calculations were done at a typical laser medium temperature of 600 degrees Kelvin. From the above derivation, it can be seen that the optical plane difference of a grating could be measured using a heterodyne technique as performed by Hutchinson (assuming that a fast enough detector is available for the wavelength and power of the laser line).

It is interesting to note that the frequency difference between polarization modes depends on the angle of reflection and type of grating used. A resonator could be designed where the frequency difference between the polarization modes is continuously variable and controlled by the angle of incidence on the primary grating. This resonator design would allow more flexibility in the frequency difference than the design used by Hutchinson which has only a fixed frequency difference for a specific grating, resonator, wavelength combination.

CHAPTER 3

DUAL LINE INTERACTION

In the previous chapter, it was shown how two laser lines (and only two) were made to operate simultaneously. If the two chosen lines have no common lasing level then there will be little or no interaction between them, and both lines will operate independently. However, if the two lasing lines do share a level, either in competition or in cascade, then the effect of the interaction can be utilized to obtain characteristics of the levels involved.

In this chapter, a model of two-line coupling is described. From the model, a measure of the two-line coupling can be derived and expressed as a constant. The relative polarization of the two-line effect on the coupling is also explained.

3.1 MODEL OF COUPLED TRANSITIONS

The different types of coupled transitions that share the same level can be seen in figure 3.1 where cascade and competitive transitions are shown.

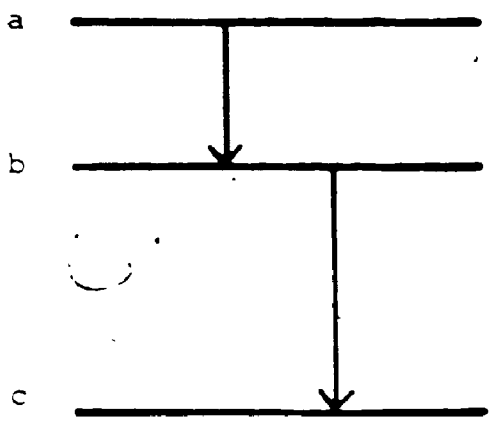

(a) Cascade

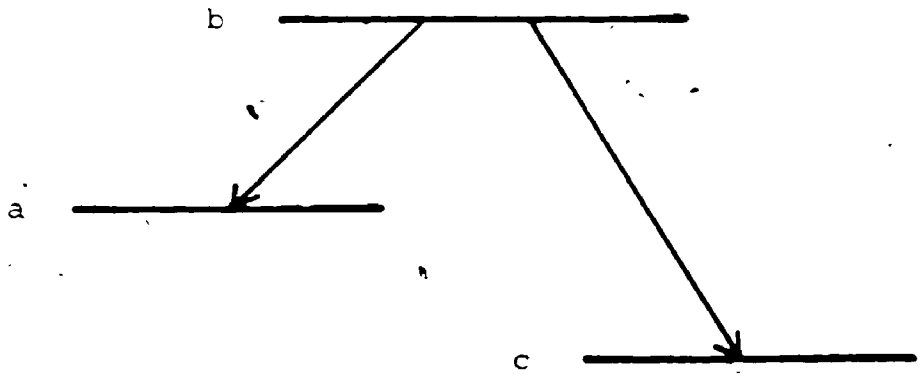

(b) Competitive

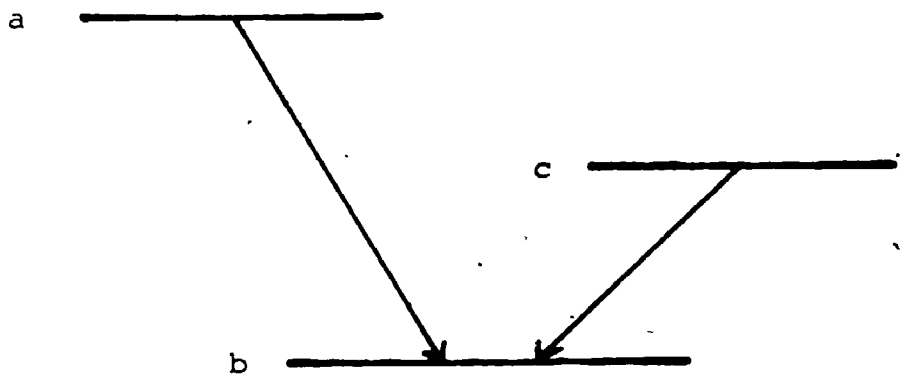

(c) Competitive

Figure 3-1
Types of Coupled Transitions

A model for the coupled transition has been derived from a semi-classical treatment of the problem (Najmabadi et al., 1975). This model is an extension of Lamb's semi-classical derivation of competition between two modes in a two level transition (Sargent et al., 1975). An outline of the derivation of the model can be found in Appendix A.

Since all the coupled lines used in the experiment were competitive types, the coupling equations used are for competitive lines. The equations can be easily adapted to cascading transitions by inverting the sign of the coupling coefficient.

Since the transition rate in laser action (stimulated emission) is related to the line intensity in the lasing medium (electric field strength squared), it is natural that the coupling is expressed as a constant multiplied by the intensity of the other line. The coupling takes the following form (Najmabadi et al., 1975):

$$\dot{I}_1 = I_1(\alpha_1 - \beta_1 I_1 - \theta_{12} I_2) \quad (3.1\text{-}1)$$

$$\dot{I}_2 = I_2(\alpha_2 - \beta_2 I_2 - \theta_{21} I_1) \quad (3.2\text{-}2)$$

where α_1 and α_2 are the net gains of the laser for the transition 1 and 2, β_1 and β_2 are the saturation parameters of the transition 1 and 2, and θ_{12} is the cross saturation that couples the intensity of transition 2 to transition 1, and θ_{21} couples transition 1 to 2.

The explicit forms of α_1, α_2, β_1, β_2, θ_{12} and θ_{21} involving the electric dipole matrix coefficient, population inversion, frequency offset of resonator modes from the transition line centre, decay rates of laser levels, Q's of resonator modes and frequencies of the laser transitions can be found in the paper by Najmabadi et al and in Appendix A.

For the coupled laser lines the steady state intensity, $\dot{I}_{1(2)} = 0$, can be found from equations 3.1-1 and 3.1-2 to be

$$I_1 = \alpha_1/\beta_1 - (\theta_{12}/\beta_1)I_2 \qquad (3.1\text{-}3)\ .$$

$$I_2 = \alpha_2/\beta_2 - (\theta_{21}/\beta_2)I_1 \qquad (3.1\text{-}4)\ .$$

Hence

$$I_1 = \alpha_1/\beta_1 - (\alpha_2\theta_{12}/\beta_1\beta_2) + (\theta_{12}\theta_{21}/\beta_1\beta_2)I_1$$

$$I_2 = \alpha_2/\beta_2 - (\alpha_1\theta_{21}/\beta_1\beta_2) + (\theta_{21}\theta_{12}/\beta_1\beta_2)I_2$$

so that

$$I_1 = (\alpha_1'/\beta_1)/(1-C)$$

$$I_2 = (\alpha_2'/\beta_2)/(1-C)$$

where α_1' and α_2' are defined by

$$\alpha_1' = \alpha_1 - \theta_{12}\alpha_2/\beta_2$$

$$\alpha_2' = \alpha_2 - \theta_{21}\alpha_1/\beta_1$$

and where a coupling constant, C, between the two transitions is (Sargent et al., 1974, chapter 9-2)

$$C = \theta_{12}\theta_{21}/\beta_1\beta_2$$

This coupling constant is a measure of the coupling between the two transitions and its value will determine whether the two modes can simultaneously lase or not. In the case of weak coupling, $C < 1$, one or the other or both lines

can lase. When C = 1 the coupling is neutral, and when C > 1 the coupling is strong and one or the other lines will not lase (Sargent et al., 1975, Najmabadi et all, 1975).

For a homogeneous standing wave laser with the resonator modes at line centre, Najabadi et al. calculated the value of a simplified version of C as

$$C = (4/9)(\gamma_a\gamma_c)/(\gamma_b+\gamma_a)(\gamma_b+\gamma_c)$$

where γ_i is the decay constant of the the transition energy level i. The simplification made is that there is no interaction between the uncoupled level, a and c in figure 3.1. Any transition between these two levels usually involves a quadrupole interaction.

In many lasers the values of the gain and saturation coefficient are difficult or impossible to obtain, but the coupling coefficient can be measured, if the laser design allows both single independent mode operation of both lines as well as simultaneous line operation. The following derivation shows how.

If the laser is made to lase on only line one (1), then $I_2 = 0$ and the single mode steady state intensity of line one (I_1) takes the form (Sargent et al., 1974)

$$I_1 = \alpha_1/\beta_1$$

and similarly the single line steady state intensity of line

two (I_2^1) takes the form

$$I_2^1 = \alpha_2/\beta_2.$$

The equations for the coupled equations, 3.1-3 and 3.1-4 then can be rewritten as follows

$$I_1 = I_1^1 - (\theta_{12}/\beta_1)I_2$$

$$I_2 = I_2^1 - (\theta_{21}/\beta_2)I_1$$

The expression can be rearranged as

$$(\theta_{12}/\beta_1) = (I_1^1-I_1)/I_2$$

$$(\theta_{21}/\beta_2) = (I_2^1-I_2)/I_1$$

so that

$$C = \theta_{12}\theta_{21}/\beta_1\beta_2$$

becomes

$$C = [(I_1^1-I_1)/I_1][(I_2^1-I_2)/I_2]$$

Thus to measure the coupling constant between two laser transitions, the intensities of the two lines are measured separately (single line operation) and then measured combined (both lines lasing). The coupling constant is the product of fractional difference between the two modes with the coupled intensities as the standard.

As described in chapter 2, the MGG laser allows both single line as well as simultaneous operation of two laser lines so that the coupling constant for a pair of coupled lines can be measured with an MGG laser. Also, since the MGG resonator controls the relative polarization of the two lines (parallel or perpendicular to each other), the dependence of the coupling constant upon the relative polarization can be

found.

3.2 MAGNETIC SUB-LEVEL COUPLING

In the preceding derivation, each energy level in the laser transitions was considered as a single state, that is non-degenerate. With molecules that have non-zero angular momentum J (or some spin value) each energy level possesses 2J+1 degenerate magnetic sub-levels, m. The characteristic values of the angular momentum, J, and the magnetic sub-levels, m,are integral (or half-integral in the case of spin). The value of J is usually not bounded and is positive while the value of m is bounded between $-J < m < J$.

When a transition occurs between two energy levels of a molecule, its probability depends not only on the perturbing force acting on the molecule, such as the electric field in stimulated emission, but also on the value and change of J and m. The transition rules for electric dipole transitions for polyatomic molecules are $\Delta J = \pm 1, 0$, $\Delta J = 0$ and $J = 0$ is forbidden, and $\Delta m = \pm 1, 0$. The transition probability coefficient corresponding to the angular momentum part of the interaction (Wigner-Eckart theorem) can be found in many quantum theory texts. (Condon and Shortley, 1935, p.61, Sobel'man, 1972, p.85).

In an ensemble of molecules the magnetic sub- level population of both lasing levels are evenly distributed

before lasing takes place. When lasing commences, there is a distribution of sub-levels participating in the lasing activity depending on the magnitude of the sub-level transition probability. That is, the lasing will occur mainly in the population whose transition probability, dependent on the magnetic quantum number, is largest. This creates a magnetic sub-level population redistribution of both the upper and lower levels. Some redistribution of magnetic sub-levels also occurs due to collisions.

When a laser is made to operate on two lines that share a common level, the magnetic sub-level distribution of each line is an important factor in the degree of coupling that will occur between the two lines. This coupling effect due to the above mentioned distribution can be accounted for by an extra coupling coefficient, C', that multiplies the single state coupling constant (Khayutin, 1979a, Melekhin and Melekhina, 1973). Obviously, the maximum and minimum values of C' are 1 and 0 respectively.

For example, two lines will have maximum coupling when they share the upper levels, both transitions have the same upper J value, and the polarization of the electric field of both transition modes are in the same direction (C' = 1). However, the coupling will be smaller (C' < 1) if the polarization of the lines are perpendicular to each other because they are not competing as much for the same magnetic

sub-level population.

As mentioned before, the distribution depends both on the angular momentum and magnetic quantum number value and their change. Transitions that are linearly polarized are called π transitions and correspond to $\Delta m = 0$ while those transitions that are right and left circularly polarized are called σ_+ and σ_- transitions respectively and correspond to $\Delta m = +1$ and $\Delta m = -1$ respectively. In figure 3.2, the relative transition distributions are presented for the combinations of $\Delta J = \pm 1, 0$ and of π and σ_+ transitions, where $J = 10$ for the lower level. The distributions of the σ_- transitions are the mirror images of the σ_+ distribution.

$$\sigma_-(m) = \sigma_+(-m)$$

The σ_+ and σ_- distributions are needed for calculating the C' coefficient not only when one or the other or both transitions emit circularly polarized light but also when the two coupled lines are linearly polarized perpendicular to each other. This can be done with a combination of the quantum operator for the circularly polarized transition as outlined below.

The principal quantum axis, often designated as the z axis, can be assigned to be the plane of polarization of the first line. There are three independent quantum operators, T_0, T_+, T_-, for electric dipole transitions (Sobel'man,

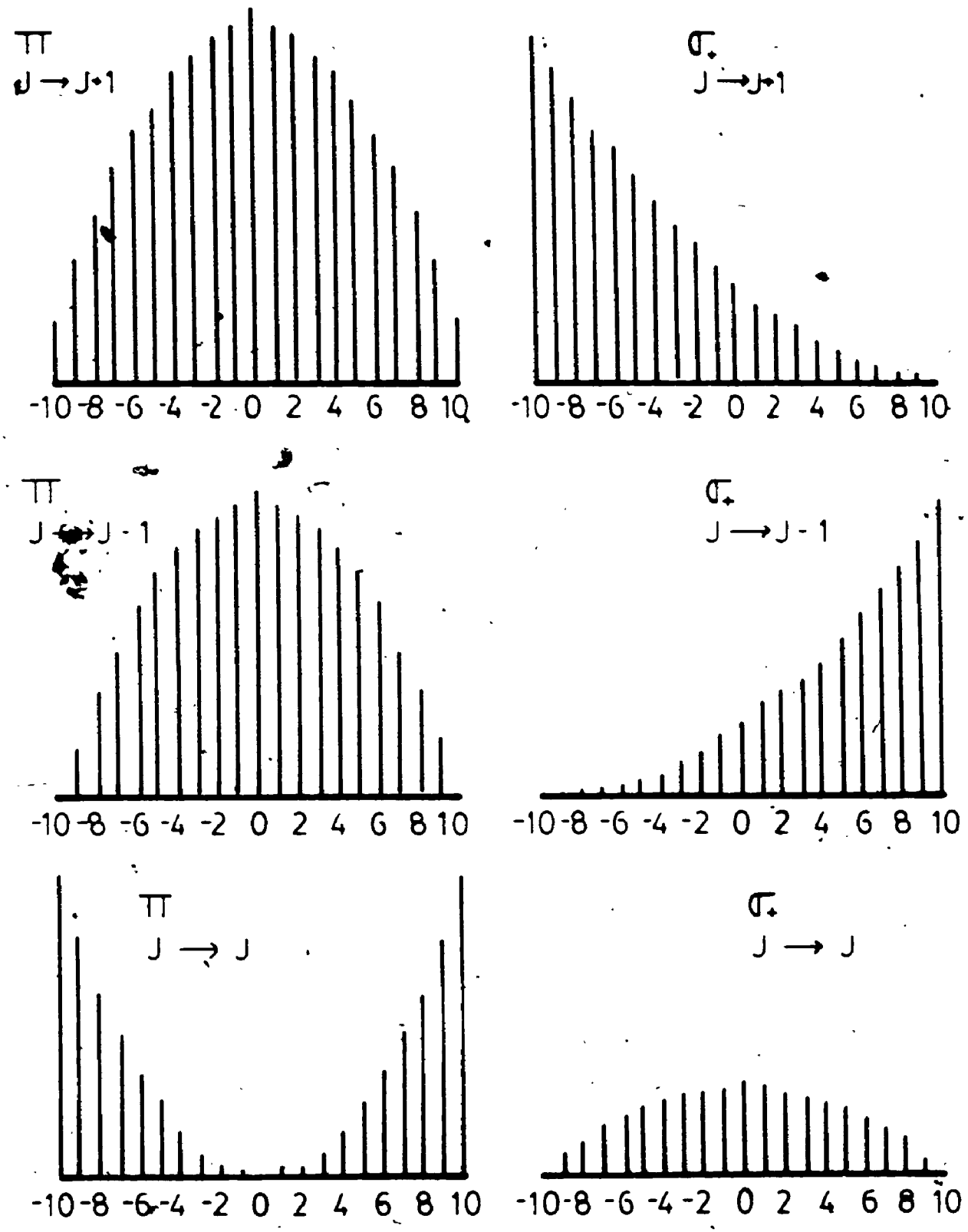

Figure 3-2
Distribution of Relative Intensities for Π and σ_+ Transitions for $\Delta J=0,+1$ (from Melekhin and Melekhina, 1973)

1972). The quantum operator T_o corresponds to transitions where $\Delta m = 0$ and $T_{\pm}$ to $\Delta m = \pm 1$. The operators $T_{\pm}$ has vector form $\hat{x} \pm i\hat{y}$. It is easy to see that an operator can be created to describe a transition linearly polarized in the x axis by a linear combination of T_+ and T_-, $T_x = (1/2)(T_+ + T_-)$ (Condon and Shortley, 1959, Melekhin and Melekhina, 1973).

From the various distributions of π, σ_+, σ_- transitions, it is possible to get a qualitative idea of the relative coupling strength of two lines for various combinations of transition types ($\Delta J = 0, \pm 1$) and electric field polarizations. With the laser used in the experiments, the polarization of the resonator modes of the two transitions are either parallel or perpendicular to each other. If the two coupled transitions have the same ΔJ then the two lines should be more tightly coupled when their electric fields are parallel to each other, than when they are perpendicular to each other. For coupled transitions where $\Delta J_1 \neq \Delta J_2$ the opposite is true. Thus experimental measurements of the correlation allow the assessment of energy level assignments.

Expressions to calculate the magnetic coupling constant, C', are tabulated in the paper by Melekhin and Melekhina (1973) for all the various combinations of electric field polarizations (circular or linear) and ΔJ transitions. To obtain the expressions for C', Melekhin and Melekhina had to calculate two 6j expressions for the 6 different combinations

of ΔJ combined with the five different relative polarization combinations. The original formulation of the coupling (the 6j expressions) can be found in Beterov and Chebotaev (1974). An alternative derivation of C' can also be found in two papers written by Khayutin (1980, 1981).

CHAPTER 4

APPARATUS

This chapter describes briefly the water vapour laser system used in the experimental part of this study. Each section of this chapter describes a different part of the laser: the laser body itself, the gas induction system, the power supply and controls, and the laser radiation detection system.

4.1 THE LASER BODY

The laser was just over 5 meters long and was constructed of 100 millimeter I.D. Kimax glass tubing, terminated by two dissimilar optical chambers. At either end of the laser, between the laser tube and the chambers, there were glass cross sections used for gas input and output, and for housing the ground ring electrodes. At the centre of the body, there were two more glass cross sections where two cold cathodes were located. Electrically the laser was divided into two sections connected in parallel, so that an electrical discharge would ideally strike from each cathode to the ring anodes, located in the end cross sections (see figure 4.1).

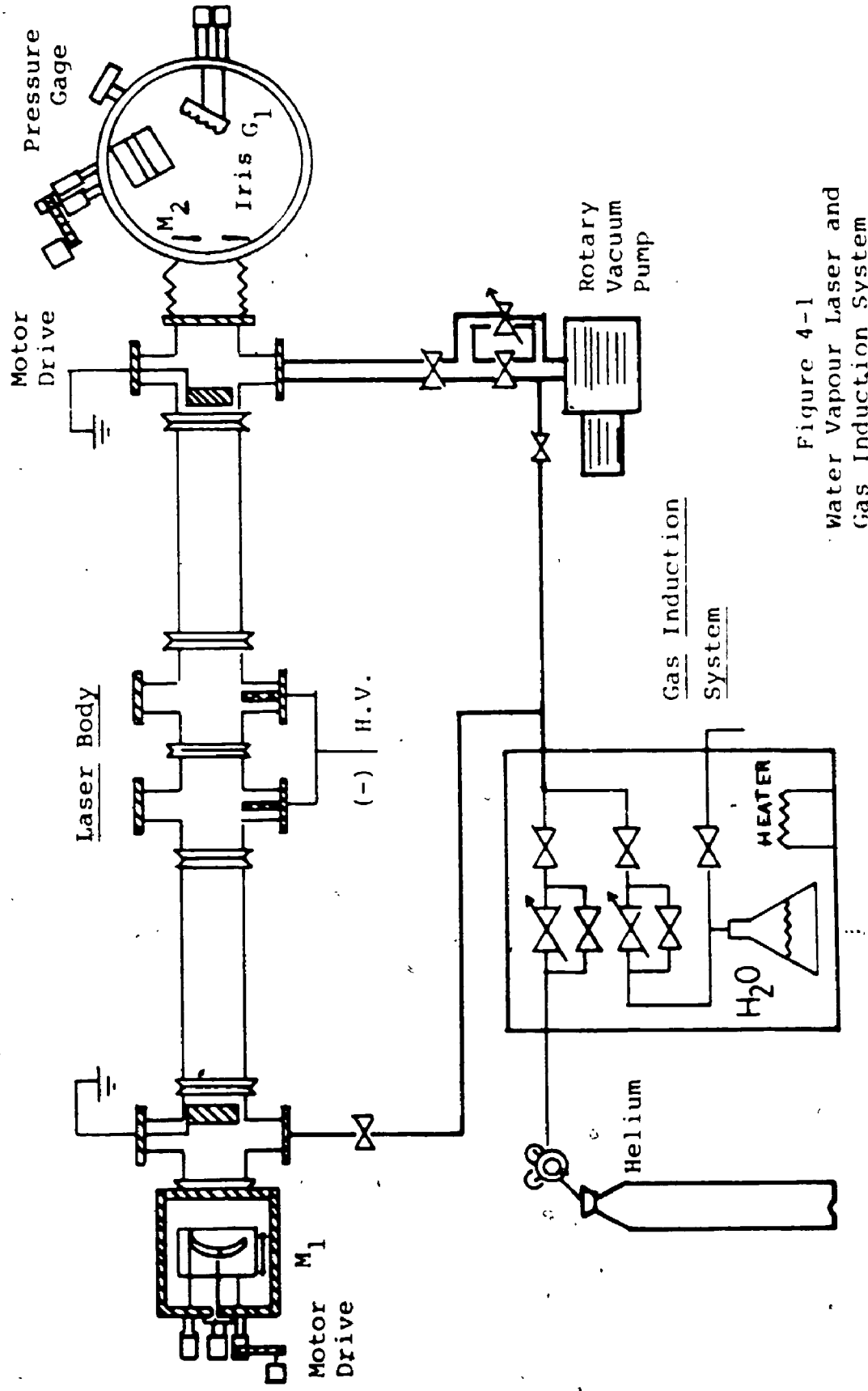

Figure 4-1
Water Vapour Laser and Gas Induction System

The central discharge configuration had two important advantages over conventional end to end electrical discharges in lasers. Firstly, both end chambers were at ground potential, facilitating adjustments that had to be done while the laser was operating. Secondly, the electrical noise produced by the central discharge configuration was low for the pulsed current discharge. In the far field, the fields generated by the two opposing pulsed discharges cancelled each other.

The cathodes were made of aluminum, and were 80 millimeters long and 25 millimeters in diameter. Each cathode had a 20 millimeters diameter hole drilled 60 millimeters into the end where the discharge originated. The cathode was attached to the glass cross section faceplate. The cathode design proved to have good discharge characteristics over previous designs, especially at low gas pressure (1 to 2 Torr of ~~helium~~).

The ring anodes at either end of the laser were made of aluminum tubing, 50 millimeters long, split down the length to ease insertion. The anodes were at ground.

Ideally the electrical discharge current should be the same for both sides of the laser. This was only found when the water vapour concentration was very even along the length of the laser, or the water vapour concentration was low. Any

imbalance in the water vapour concentration would intensify the discharge in the low water vapour pressure side. The discharge would continue to favour that side after the concentration became homogeneous or when the vapour concentration was reversed (within limits). With limited success for low to medium concentrations of water vapour, the discharge could be balanced by wrapping grounded aluminum foil to the body of the laser. This balancing technique did not work with typical helium water vapour pressure used in the experiments (4.5 Torr of helium and 1.0 Torr of water vapour). Perhaps the solution to the uneven discharge problem is to use glow discharge cathodes. The one sided discharge generated enough laser power to carry out the experiments.

The laser resonator cavity consisted at one end of a spherical 100 millimeter diameter gold over nickel mirror (mirror radius = 8 meters), M1, and at the other end by a coupled grating system. (See Appendix B for coating methods) The 100 millimeter mirror had a 2 millimeters diameter radiation coupling hole in its centre, drilled with a diamond embedded hollow drill. The mirror was held in a gimbal mount attached to a translation stage inside a cylindrical aluminum chamber 300 millimeters long, 300 millimeters in diameter. The rear access plate of the chamber had a 25 millimeter diameter polyethylene window aligned with the mirror hole. Vacuum feedthrough controls for the mirror were also located on the rear plate. The exterior micrometer used to position

the translation stage could be motor driven for constant velocity translation of the mirror.

The principal grating and the secondary optics at the other end of the laser resonator were located in a vertical aluminum cylindrical chamber, 495 millimeters in diameter and 55 millimeters in height. The bottom metal plate of the chamber was permanently attached to the cylinder, while the top was an 18 millimeters thick plate glass sheet that rested on an 'O' ring, located in a groove fabricated in the edge of the chamber. The glass plate allowed easy access to the laser optics and facilitated alignment procedures (P.A. Rochefort, 1981). The principal grating, G1, was held in a gimbal mount. A mirror, M2, or grating, G2, was used as the secondary optical element and held by gimbal mount and was attached to a translation stage. Both mirror mounts and the translation stage were adjusted with external controls. The secondary optical element (usually the grating G_2) could be rotated about the optical axis. The worm gear of the rotation device was magnetically coupled through the top glass plate of the chamber. The external micrometer for the translation stage, similar to the one used for the principal mirror, could also be motor driven.

An absorber could be placed by means of a vacuum feedthrough between the principal grating and the secondary optical element. This allowed the laser to be converted

easily from a compound MGM or MGG resonator to a MG resonator.

The design of the motor drive for both the principal mirror and the secondary optic were similar . A synchronous motor-gear, reduced to one revolution per minute (rpm), rotated the micrometer head by means of a corrugated rubber timing belt. With the available gears and micrometers, the translation stages could be driven at 17.01 microns per minute or 31.75 microns per minute. For calibration purposes, both drives had magnetically coupled relay switches that were activated once every revolution of the micrometer.

4.2 GAS INDUCTION SYSTEM

The laser used a flowing mixture of water vapour and helium. The gas mixture entered at the principal mirror chamber end and exited at the grating chamber end of the laser. The flow and pressure of the laser was controlled by a combination of needle valves for the gas inputs and for the mixed gas output. The output needle valve was usually left at one setting while the input control valves were adjusted to required partial pressures. Both the input and output needle valves had in-line on/off toggle valves to preserve settings, and valved by-pass lines for rapid evacuation. Gas flow rate for the laser at 3.3 torr (helium) and 24 degrees Celsius was $3.37X10^{-2}$ litres per second, or at STP $1.36X10^{-4}$ liters per second.

A heated box regulated to 30 degrees Celsius contained the gas induction and the water vapour delivery systems. The water vapour for the laser was drawn from the heated water held in a ~~glass~~ flask inside the box. The water at the regulated temperature had a vapour pressure of 30 torr while the laser operated with partial water vapour pressures of 0.1 to 2.0 torr. There was a separate valved inlet to the flask so that it could be refilled without having to open the box and break vacuum seals. The helium gas was delivered from a tank with a regulated pressure of 100 kPa to the helium input system.

The laser was evacuated by means of a two stage rotary vacuum pump. The rotary pump had to have the air ballast open at all times so that the water vapour did not condense into the vacuum oil and damage the pump.

A connection was provided that could by-pass the laser body and link the vacuum pump directly to the gas handling system. This allowed the direct evacuation of the helium and water vapour lines. More importantly, when the water flask had been refilled, this connection allowed the direct evacuation of dissolved gases in the water.

The gas pressure was measured using a diaphragm type pressure meter (Baratron 222 A) with a pressure range of 0.01 torr to 10.00 torr. The pressure was read from a 10 volt full

scale voltmeter. The gas pressure was measured at the grating chamber away from any electrical discharges.

4.3 POWER SUPPLY

The pulse power for the laser was supplied from a General Electric modulator originally designed to power a radar system. The modulator consisted of three parts, a variable DC high voltage supply, a power modulation unit and trigger control system (see figure 4-2).

The DC power supply was comprised of a variable three phase transformer that supplied zero to 220 volts to the high voltage transformer. The AC power from the high voltage transformer was rectified (with vacuum tube diodes) and filtered with a high voltage capacitor. The DC power supply was rated for 750 milliamperes at 12 kilovolts.

The power modulator unit consisted of a voltage doubler coil with a hold-off diode in series, a pulsed forming network to store the power and shape the output pulse, and a hydrogen thyratron high voltage switch, to deliver the power to the load. The modulator could be configured, at a setting of a switch, to deliver either a 1 or 2 microsecond rectangular pulse into a matched load. Since the laser was pumped by a gas discharge, the laser's impedance was neither constant nor well matched with the modulator output impedance. As a result, the current pulses at the 1 microsecond setting were

about 3 to 4 microseconds long, and approximately triangular in shape. The typical operational peak current and voltage for the laser with 4.5 torr of helium and 1.1 torr of water was about 600 Amperes and 25 kilovolts. The current of the modulator was measured using a special high speed current transformer mounted on the output port of the modulator (Sarjeant and Brannen, 1968 a,b). The voltage was measured with a high resistance voltage divider in parallel with the load.

The trigger control system was made up of a pulse generator and a high voltage trigger circuit. The generator used the rectified power line signal (120 Hz.) as its clock standard and the timing pulse rate was set by dividing (1 to 99 in integer steps) the clock frequency, so that the pulse generator frequency rates were integer fractions of 120 Hz.. Also, the phase of the pulses with respect to the power mains signal could be varied. Since the charging of the pulse forming network of the modulator depended on what power main phase angle the charging occurred and with the trigger circuit tied in to the power mains, the pulse to pulse power was as constant as possible. For all the experiments in this thesis the pulse rate was 30 Hz..

Because the hydrogen thyratron in the modulator needed a high voltage pulse to discharge, a high voltage trigger circuit was constructed to step up the voltage of the trigger

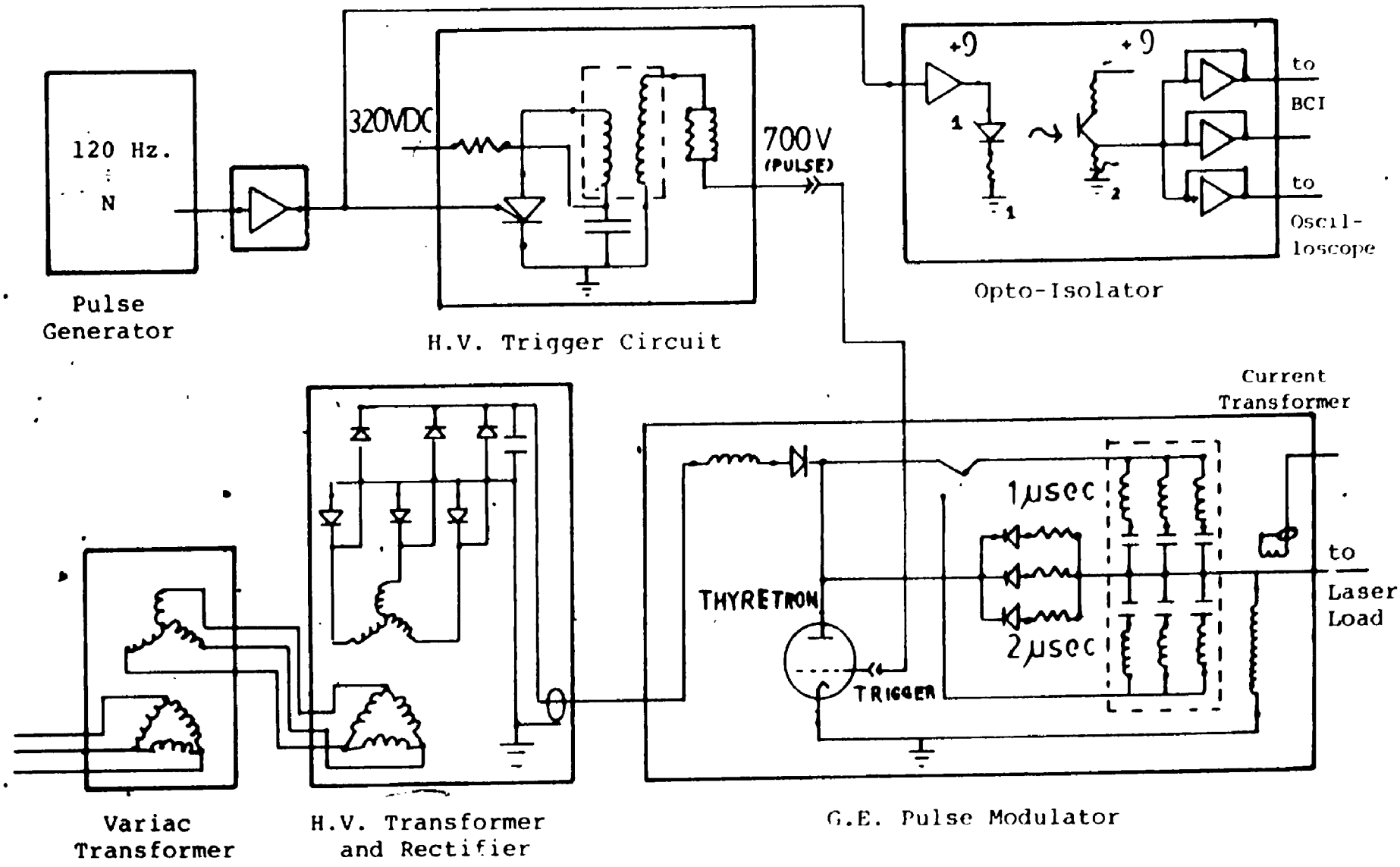

Figure 4-2
Power Supply and Control for the Water Vapour Laser

pulse from the generator.

The timing pulse was also used to trigger the detection system box car averager (BCA) and monitoring oscilloscopes. Because of the large ground loops created by the laser high peak current, the signal pulse was decoupled from the BCA and oscilloscope circuit by means of an opto-isolator.

4.4 DETECTION SYSTEM

The laser radiation was coupled out of the laser, as mentioned before, by a hole in the centre of the principal mirror and then passed through a window in the chamber. The output beam was then redirected perpendicular to the laser to a long focal length concave mirror (mirror radius = 1 metre). The concave mirror was needed because of significant beam divergence caused by the diffraction of the radiation from the hole aperture. The converging beam was then directed to one of two detection setups, depending on whether the laser was in the MGM or MGG resonator configuration.

To study the polarization interaction of the MGM laser, the detection system was designed so that the power of both polarization mode signals would be recorded simultaneously. The laser radiation was split by a silicon beam splitter, and each part passed through a polarizer and on to a detector (see figure 4.3a). The two polarizers were set at 90 degrees to each other. The polarizer set at 90 degrees was for

radiation polarized perpendicular to the principal grating rulings and the other polarizer was for parallel radiation. The two detector signals were averaged by a two channel box car averager (BCA) (P.A.R., model 162). The timing of sampling gates was adjusted to measure at the peak of the integrated laser signal (see below). The BCA time constant for both channels was about 1 second (30 laser pulses). The averaged signals were recorded on two channel chart recorders (Wanatabe, model SR652-Z).

The detection system for the MGG laser was similar to that of the MGM, except the beam splitter was replaced by a grating, and no polarizers were used (see figure 4.3b). The grating was used to diffract the two lines on to detectors. Only one grating was needed for all the pairs of laser lines investigated. The grating was blazed for 78 micrometers, had rule spacing of 100 micrometers (10 grooves/millimetre), and facet blaze angle of 23.1 degrees. The powers of the shorter wavelengths lines (26.6 and 27.97 micrometers) were measured from the second order diffraction off the grating, and the longer wavelengths were from the first order diffraction.

For all the experiments, the laser radiation was detected by a pyroelectric detector (Molectron P1-11). Since pyroelectric detectors are thermal detectors (Putley, 1980), they produce an output current proporticnal to the intensity of radiation that they absorb, and their spectral response

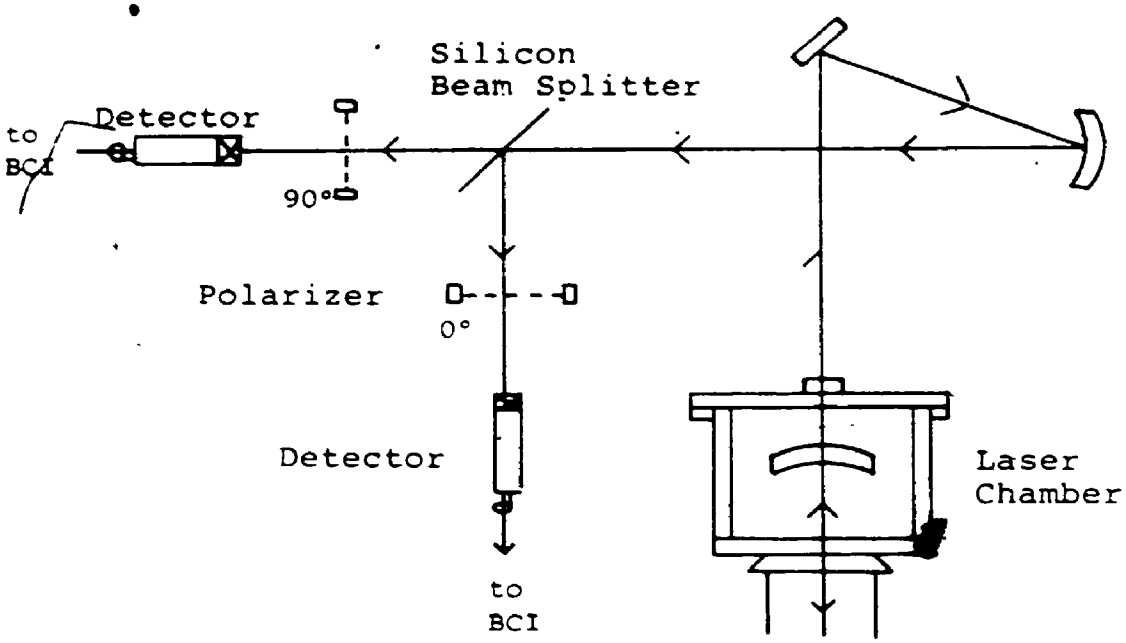

Figure 4-3 (a)
Optical Detection System used in the
Dual Polarization Experiments

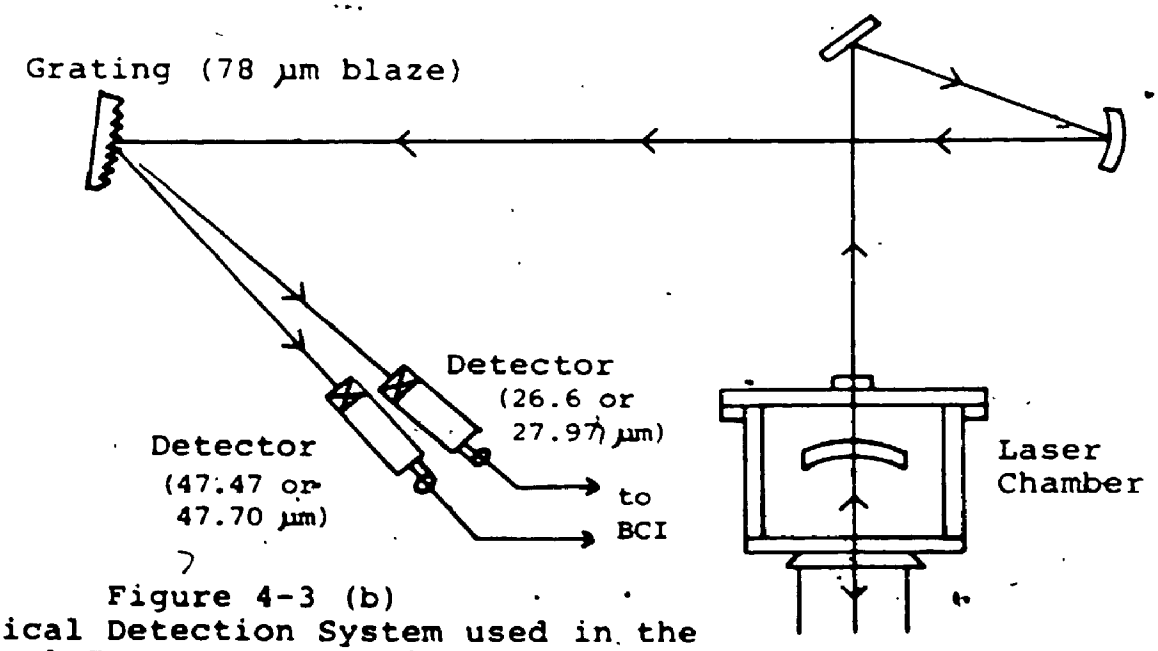

Figure 4-3 (b)
Optical Detection System used in the
Dual Frequency Experiments

Figure 4-3
Optical Detection Systems

ranges in principle from the visible to the millimetre wavelength region.

To make the detector very sensitive for very small signals, a large resistance must be used as a load resistor to the detector element. The load resistance for the P1-11 detector elements was 100 Megohms. The high frequency response of the detector was inversely proportional to the detector load time constant. The high frequency cut-off point of the detector element, resistive load combination was approximately 100 Hz., and as a result the detector system integrated very fast signals. Hence, for the short laser pulses from the water vapour laser (from 3 to 4 microseconds), the detector system operated as a pulse radiation integrator. The maximum output signal of the detector was proportional to the total energy of the laser pulse.

To reduce the acoustic noise signal, air current thermal noise (which can vary the detectors element temperature), and to limit the wavelength range sensitivity, the pyroelectric detectors are often fitted with windows. The P1-11 Molectron detector crystal is mounted inside a TO-5 transistor package with the top removed so that a window can be fitted into the opening. About half of the detectors in the laboratory were fitted with KRS-5 windows and have a detection range of .6 to 50 micrometers (Molectron, Kimmitt, 1970) and were used for single wavelength experiments at 26.6 and 27.97 micrometers.

CHAPTER 5

MIRROR-GRATING-MIRROR EXPERIMENTS AND RESULTS

The first experiment with a mirror-grating-mirror (MGM) compound grating resonator was done by Sarjeant and Brannen in 1970. They reported that radiation, parallel or perpendicular relative to the principal grating's lines was emitted from the laser with the polarization depending on the position of the secondary mirror, M_2. (see figure 2.3) (Sarjeant and Brannen, 1970).

The properties of an MGM laser were further studied in detail for this thesis. The interaction of the two modes and the lasing medium with respect to the length of both the principal and secondary cavities were investigated.

5.1 MGM EXPERIMENTAL DESIGN AND METHODOLOGY

Before any experiments were done, the laser system was activated for at least an hour before commencing the experiment. The laser was pulsed at 30 Hz. pulse repetition rate, the high voltage supply was set at 12 kilovolts and the modulator was set for 1 microsecond pulse width. The helium partial pressure was set at 4.6 Torr (cold, no electrical

discharge) , and was very stable over the long term. The water vapour partial pressure was adjusted until the total pressure was 5.3 Torr (cold). During the warm up period, optical elements could be aligned.

The MGM resonator was aligned in two steps. First, the principal grating was aligned for maximum power on the fundamental mode with a small iris aperture. Then the secondary mirror horizontal and vertical axis tilt angles were set. The initial horizontal tilt angle of the mirror was set from the measured horizontal angle of the principal grating with the bottom of the chamber. The initial vertical tilt of the mirror was set by aligning the mirror with a transparent template set upon the glass top of the chamber. The secondary mirror was then adjusted until a parallel polarized signal was found.

The first MGM experiments where done with both principal and secondary mirrors moving simultaneously with one of the mirrors moving much faster than the other. These results were used to get an initial feel for the apparatus. For the results shown in figures 5.1 the two polarized signals were recorded simultaneously while the primary mirror, M_1, was translated continuously,with the secondary mirror, M_2, at a fixed position. After sufficient translation of the primary mirror, the secondary mirror was moved by a set amount to a new position. For the results presented in figure 5.2 the

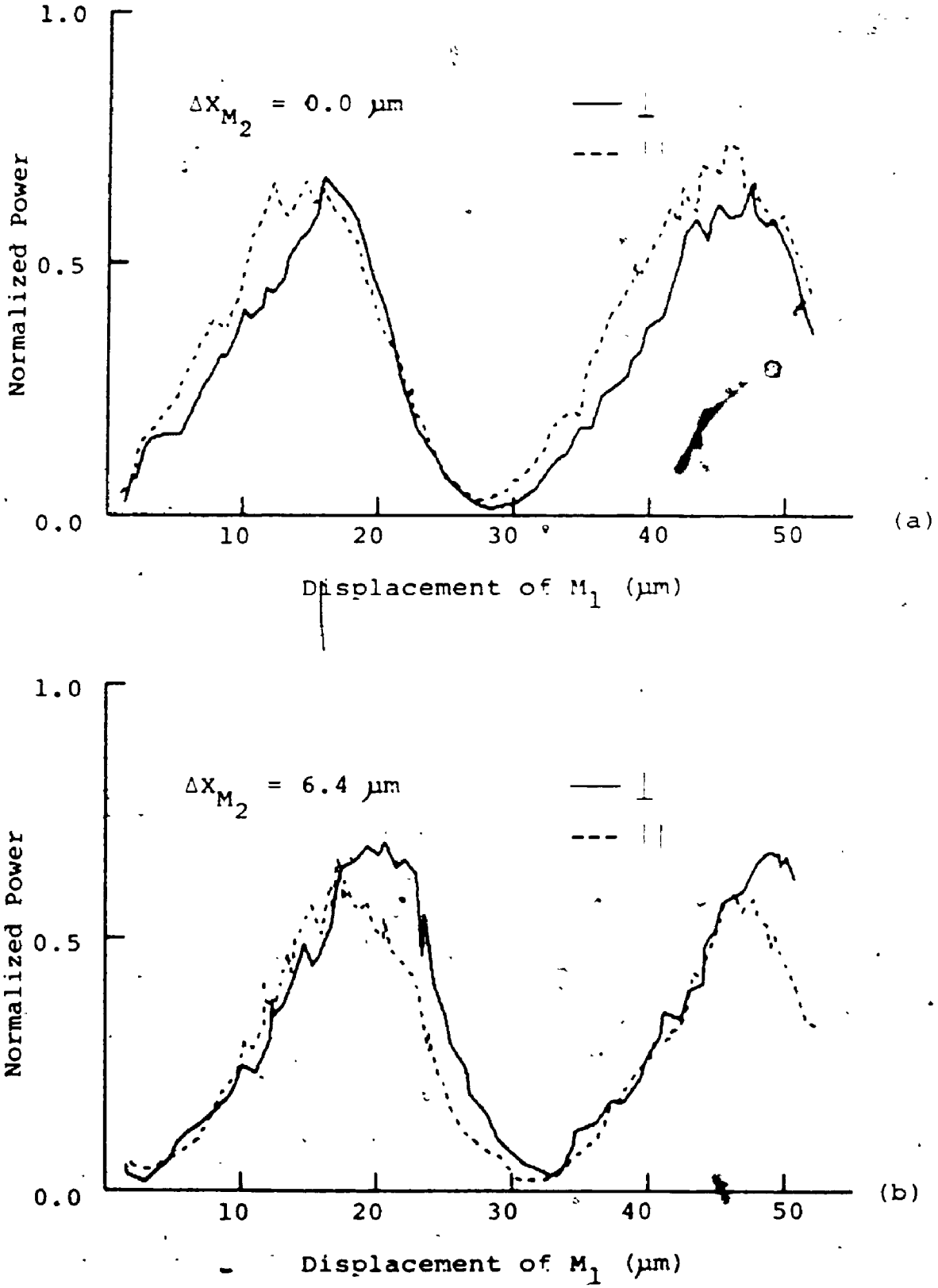

Figure 5-1
Normalized Power of the Two Polarization Modes
Versus the Displacement of M_1

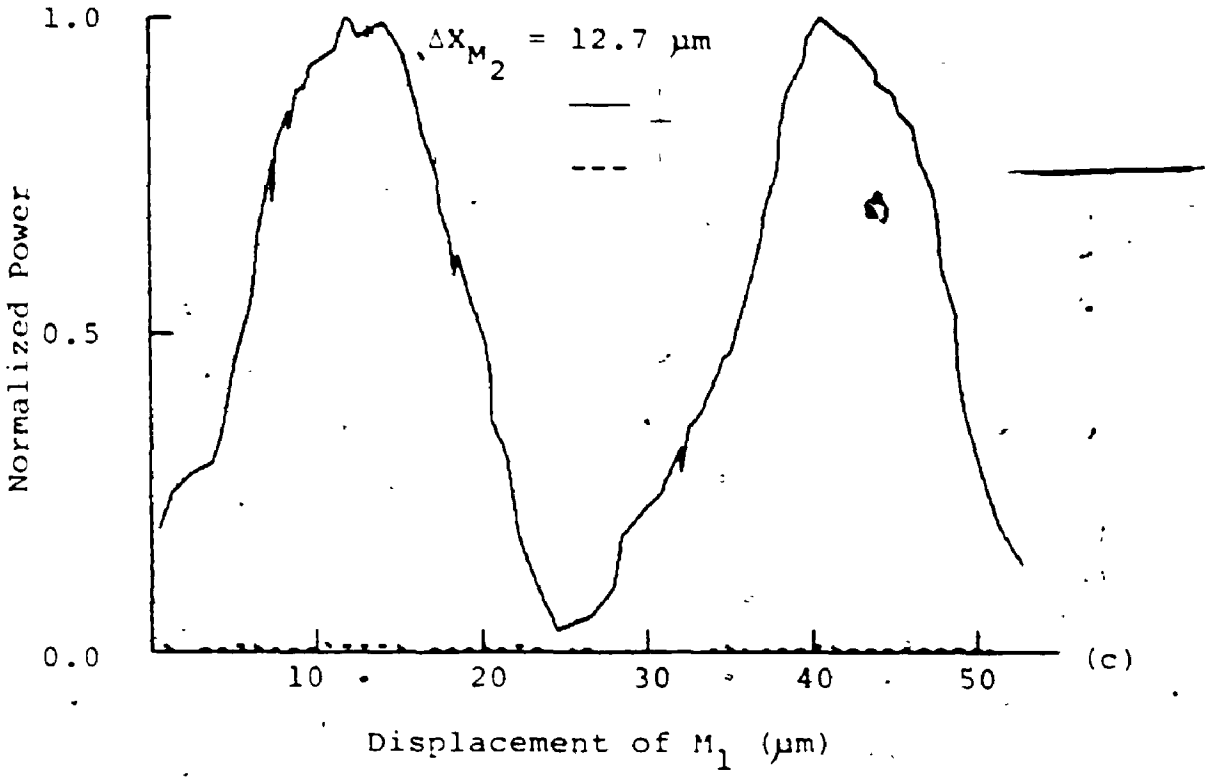
1.0
0.5
0.0
Normalized Power
ΔX_{M_2} = 12.7 μm
10
20
30
40
50
Displacement of M_1 (μm)
(c)

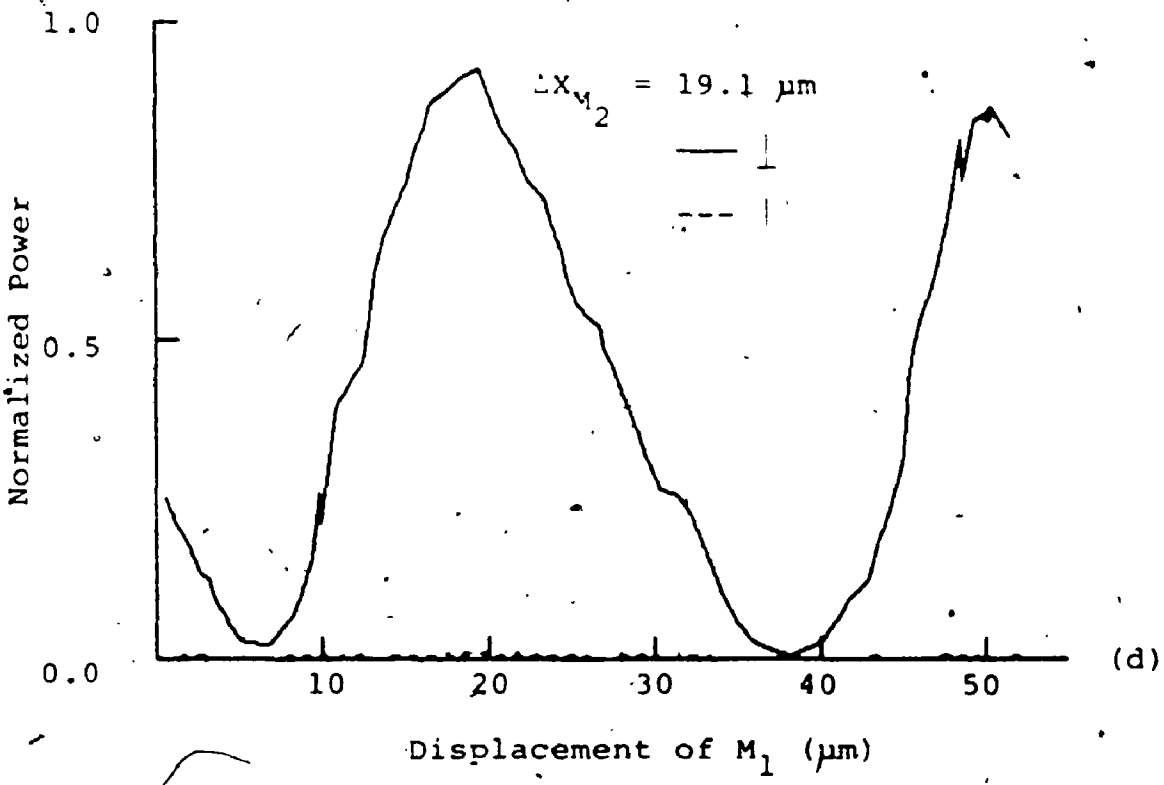
1.0
0.5
0.0
Normalized Power
ΔX_{M_2} = 19.1 μm
10
20
30
40
50
Displacement of M_1 (μm)
(d)

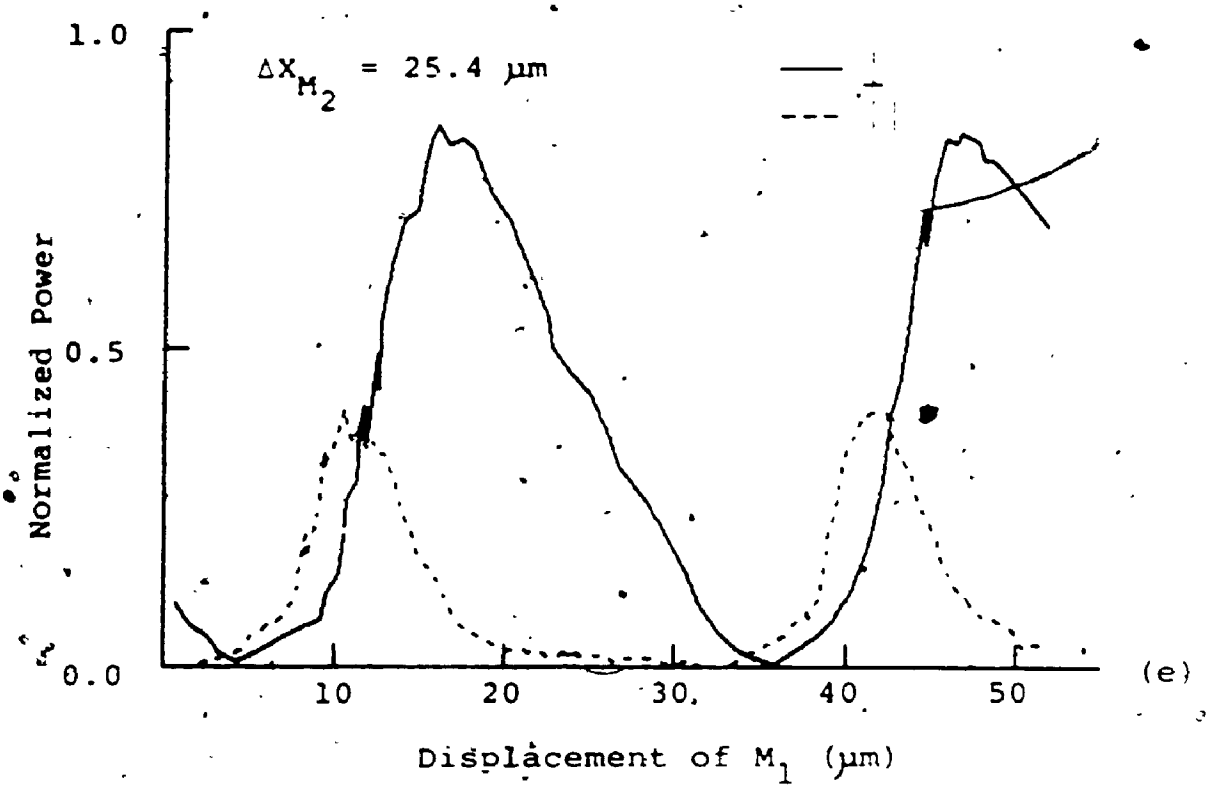
1.0
0.5
0.0
ΔX_{M_2} = 25.4 μm
⊥
∥
Normalized Power
10
20
30
40
50
Displacement of M_1 (μm)

(e)

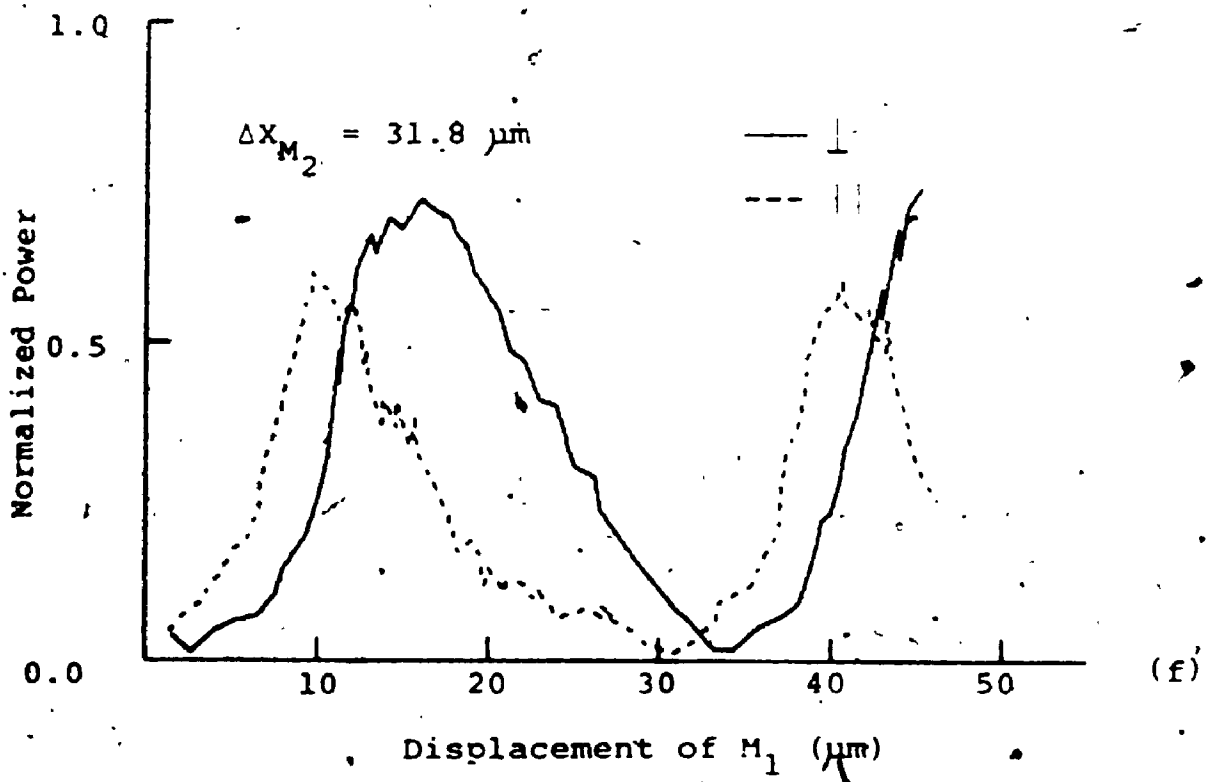
1.0
0.5
0.0
ΔX_{M_2} = 31.8 μm
⊥
∥
Normalized Power
10
20
30
40
50
Displacement of M_1 (μm)

(f)

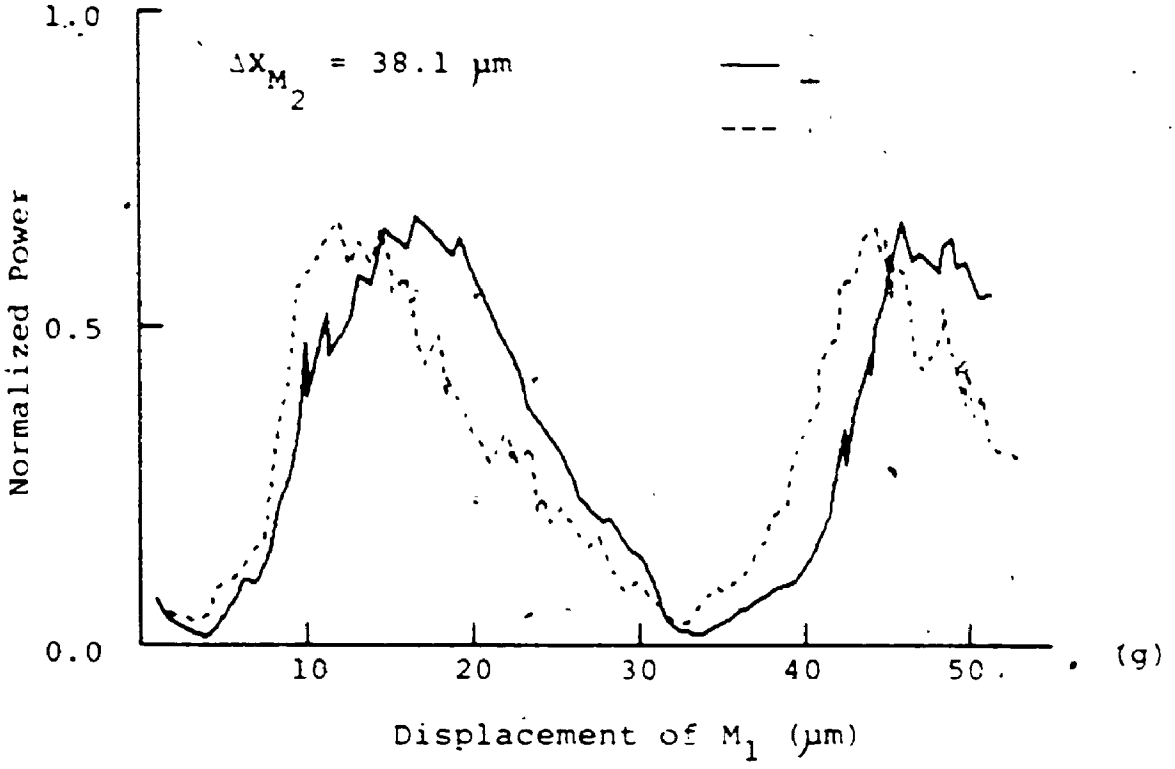
1.0
ΔX_{M_2} = 38.1 μm
Normalized Power
0.5
0.0
10
20
30
40
50
Displacement of M_1 (μm)

(g)

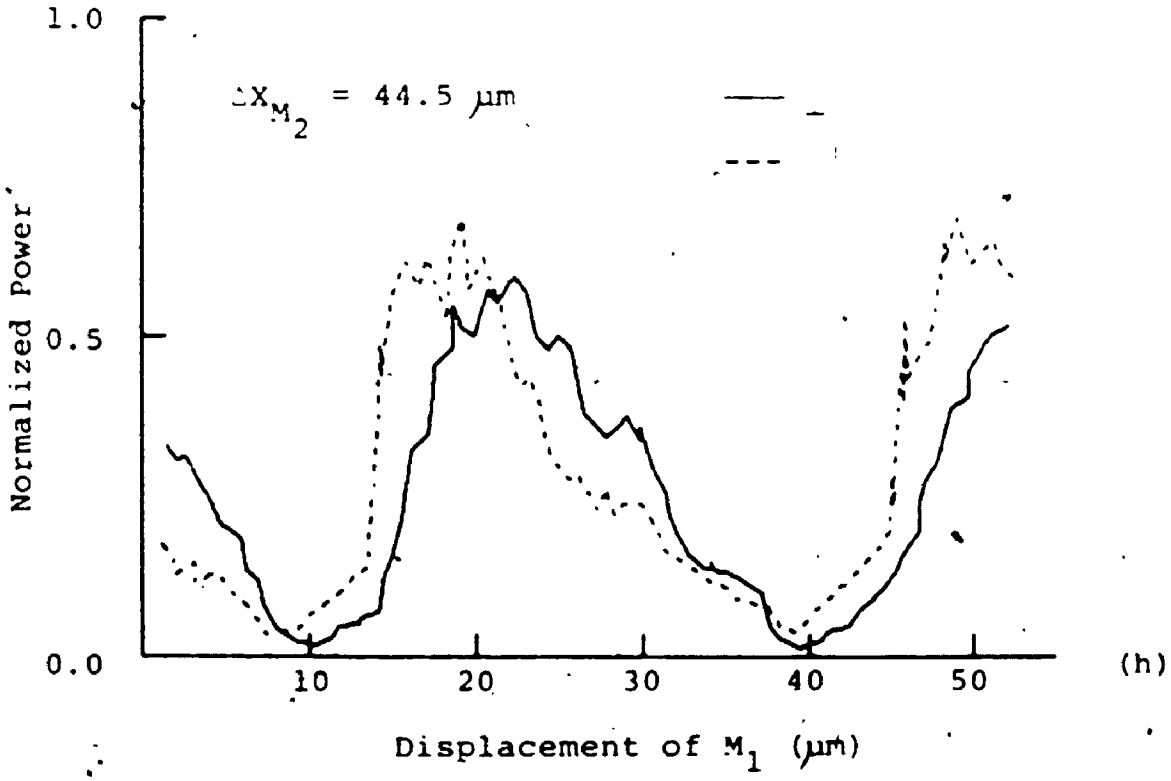
1.0
ΔX_{M_2} = 44.5 μm
Normalized Power
0.5
0.0
10
20
30
40
50
Displacement of M_1 (μm)

(h)

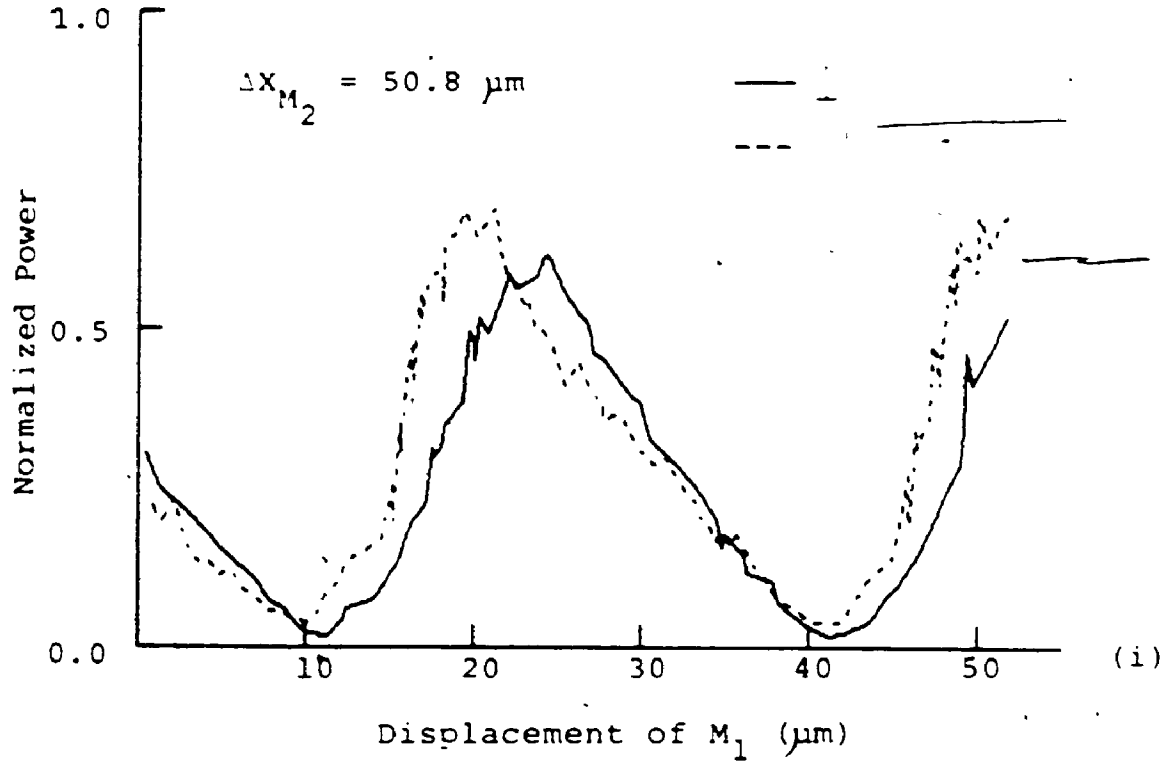
1.0
0.5
0.0
Normalized Power
ΔX_{M_2} = 50.8 μm
10
20
30
40
50
Displacement of M_1 (μm)

(i)

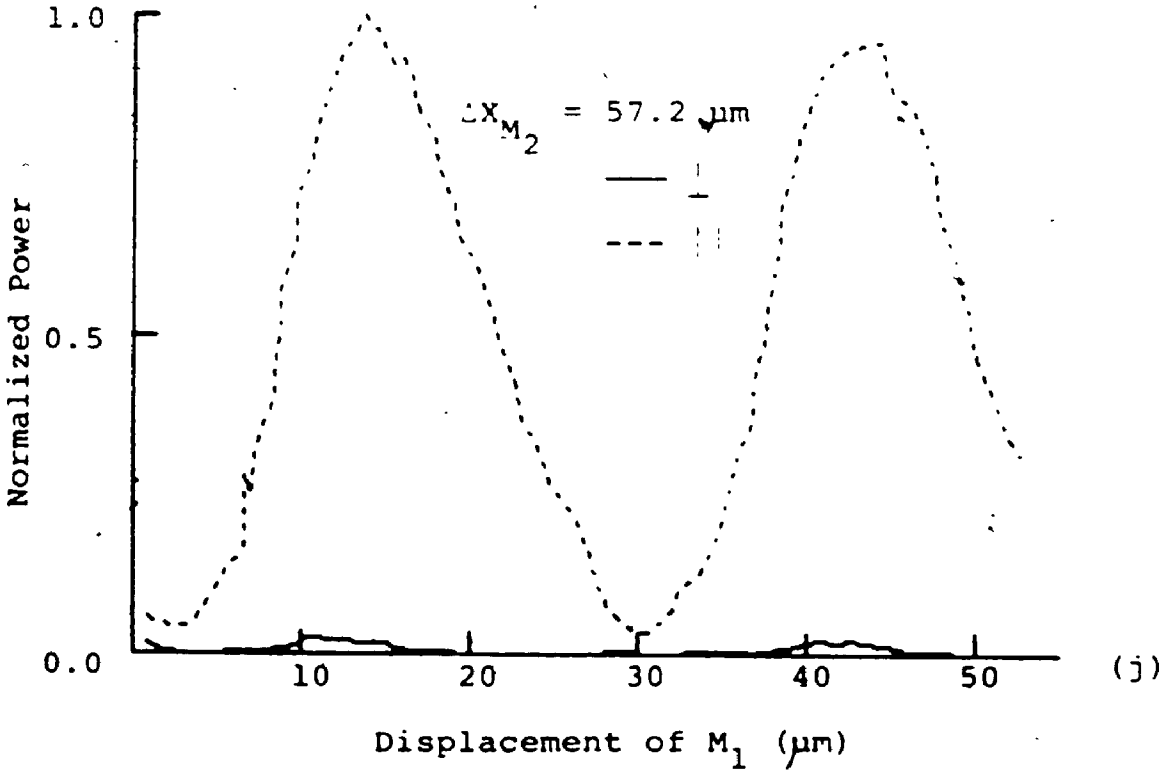
1.0
0.5
0.0
Normalized Power
ΔX_{M_2} = 57.2 μm
10
20
30
40
50
Displacement of M_1 (μm)

(j)

secondary mirror was translated continuously, while the primary mirror was moved in steps.

5.2 MIRROR-GRATING-MIRROR EXPERIMENTAL RESULTS

The preliminary experiments with the MGM resonator were done with the 27.97 micrometer laser line. This line is one of the strongest of all the water vapour lines (Benedict et al., 1969). However, difficulties were encountered with the experimental results.

The difficulties arose because the Doppler broadening of 27.97 micrometer water vapour line was of the order of the free spectral range of the primary cavity of the laser (frequency difference between adjacent longitudinal modes). The Doppler broadening of the 27.97 micrometer line at a typical discharge temperature of 600 Kelvin was 44.4 MHz (FWHM), and the free spectral range of the 4.4 meter long laser was 34 MHz. Therefore, two longitudinal modes could be within the gain curve of the 27.97 micrometer line and could lase simultaneously. This was verified by the 50% modulation of the 27.97 micrometer line laser power as the principal mirror of a simple MG resonator was translated.

The 118.6 micrometer water vapour line was chosen for further experiments with the MGM resonator. The 118.6 micrometer Doppler broadening under similar conditions as above was 10.5 MHz.(FWHM). The homogeneous pressure broade-

ning of the 118.6 micrometer line was approximated to be 27 MHz. The homogeneous line width was calculated from the pressure broadening approximation of 5 MHZ/Torr. Thus only one longitudinal mode at a time was within the 118.6 micrometer line gain curve resulting in a nearly 100% modulation of the 118.6 micrometer line with translation of the primary mirror in a simple MG resonator.

There were a few drawbacks in working with the 118.6 micrometer line. The 118.6 micrometer laser power was not as strong as the 27.97 micrometer line. The 118.6 micrometer power was also limited by simultaneous lasing of the 39.69 micrometer line, as mentioned in chapter 2. The 39.69 micrometer line lased on the third order Littrow configuration. If the concentration of water vapour got too great, $P_{H2O} > 1$ Torr, or if the current was too high, then the 39.69 micrometer line would start to lase, and would almost completely suppress the power of 118.6 micrometer line. With these limits, the optimum operating conditions for the 118.6 micrometer line could not be reached. To verify that only the 118.6 micrometer line was lasing, the power modulation period was observed with respect to the translation of the principal mirror (MG resonator).

As the final difficulty encountered, the background noise level of the detectors was greater for the 118.6 micrometer line than for the 28 micrometer line, because the

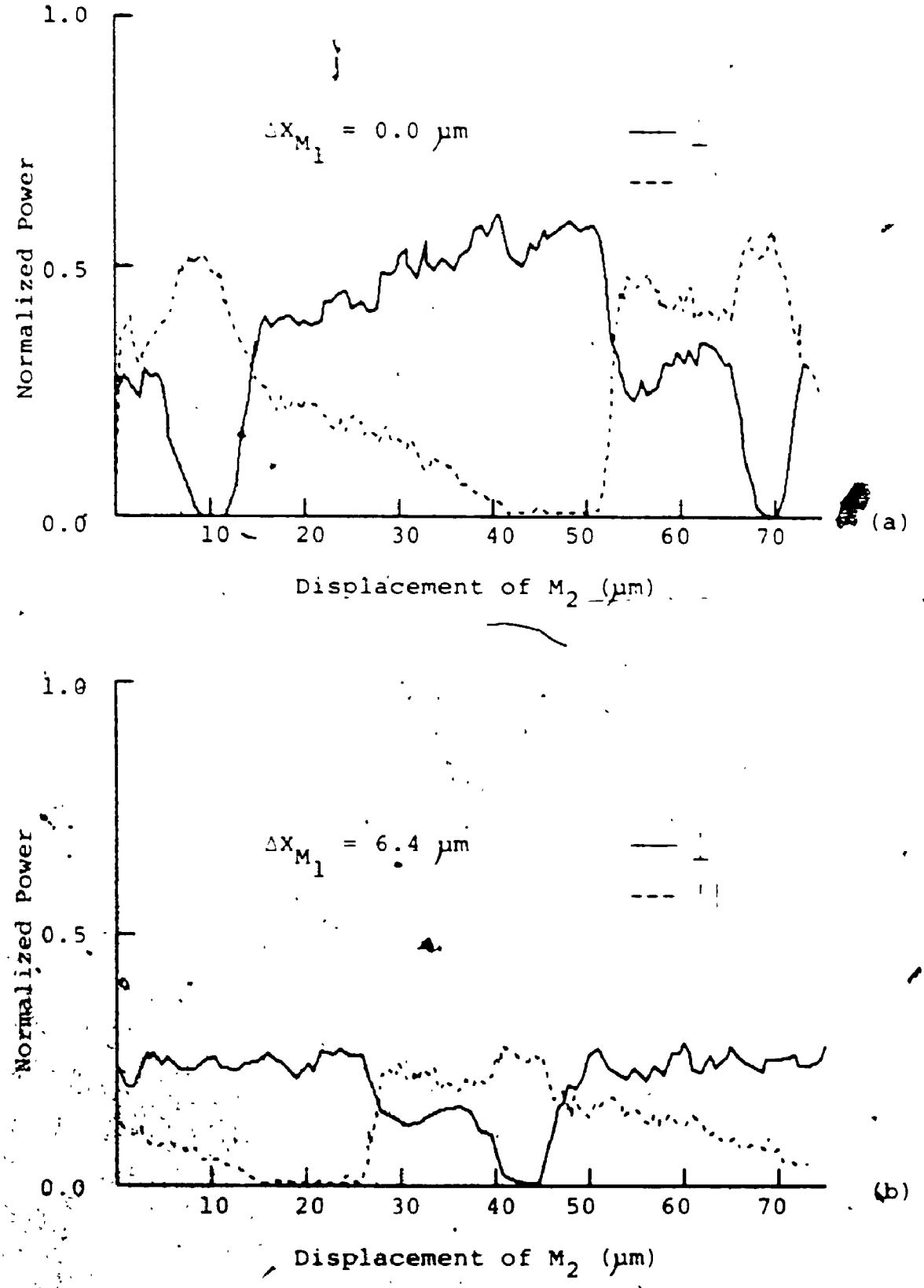

Figure 5-2
Normalized Power of the Two Polarization Modes
Versus the Displacement of M_2

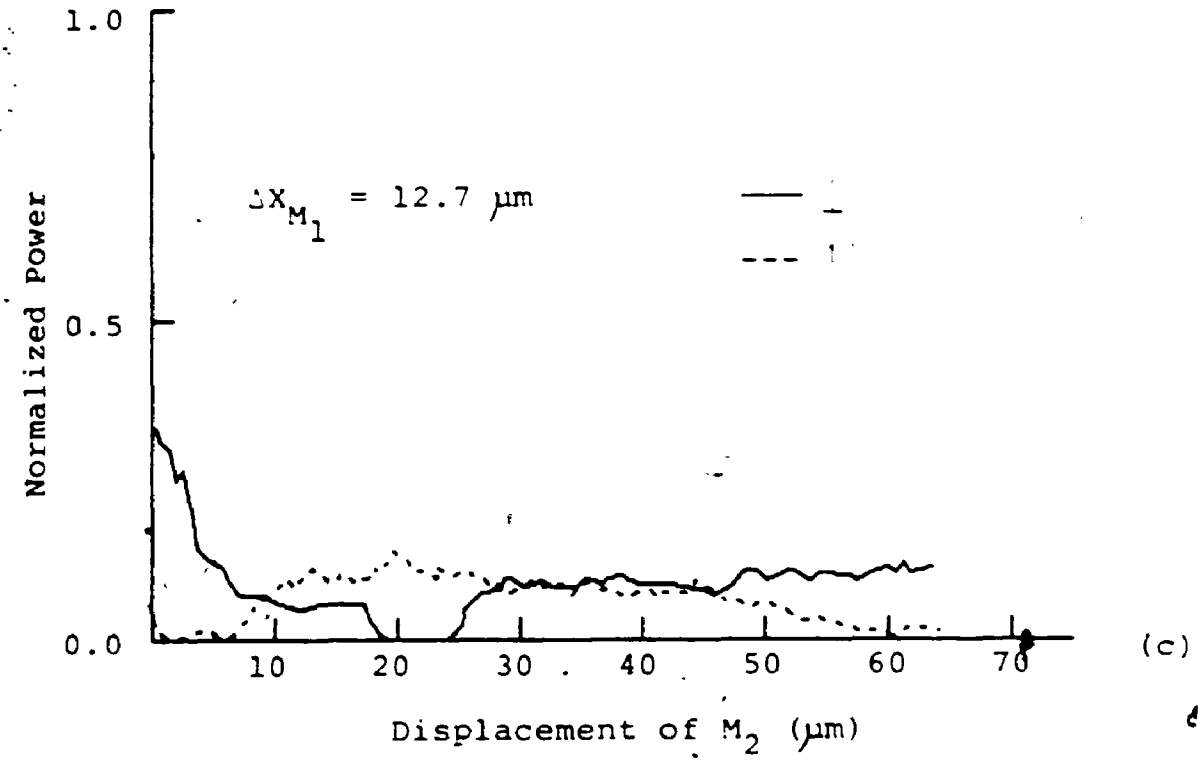
1.0
0.5
0.0
Normalized Power
ΔX_{M_1} = 12.7 μm
10
20
30
40
50
60
70
Displacement of M_2 (μm)

(c)

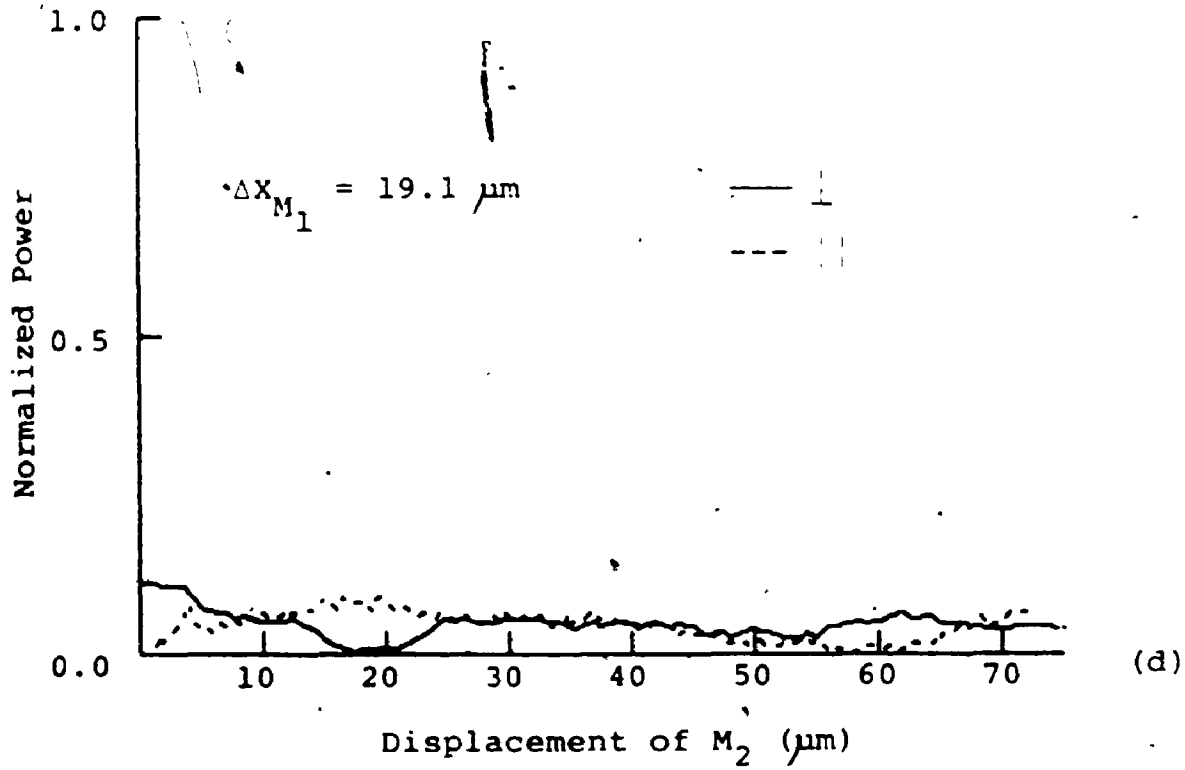
1.0
0.5
0.0
Normalized Power
ΔX_{M_1} = 19.1 μm
10
20
30
40
50
60
70
Displacement of M_2 (μm)

(d)

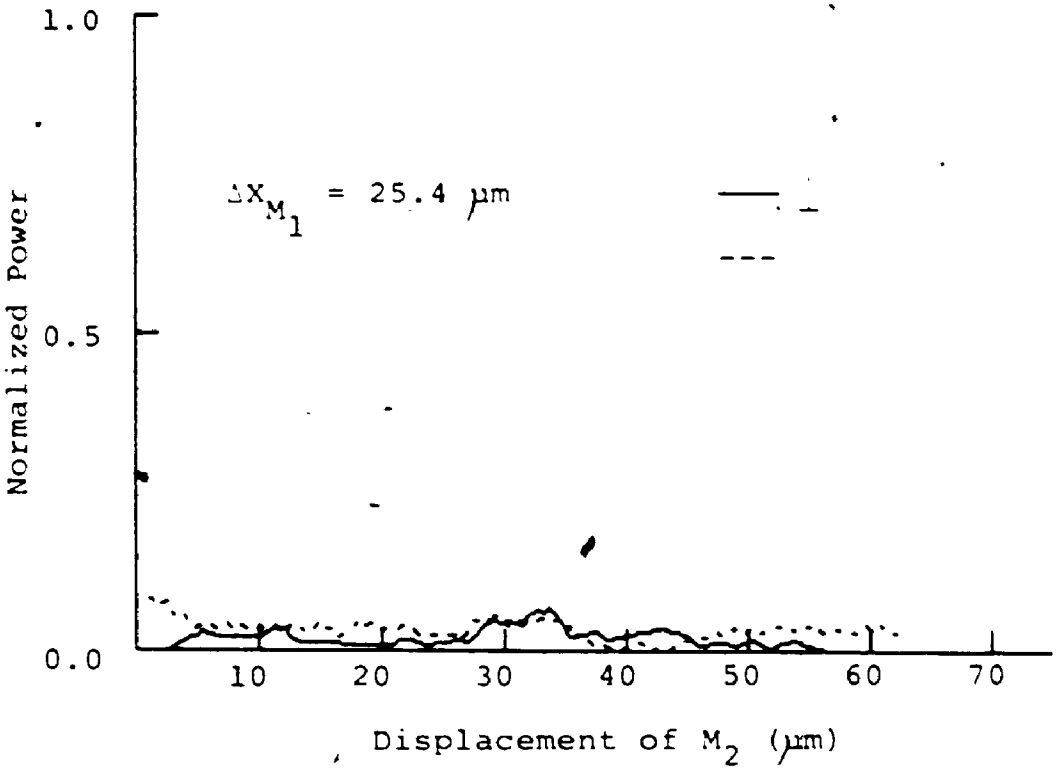
1.0
0.5
0.0
Normalized Power
ΔX_{M_1} = 25.4 μm
⊥
||
10
20
30
40
50
60
70
Displacement of M_2 (μm)

(e)

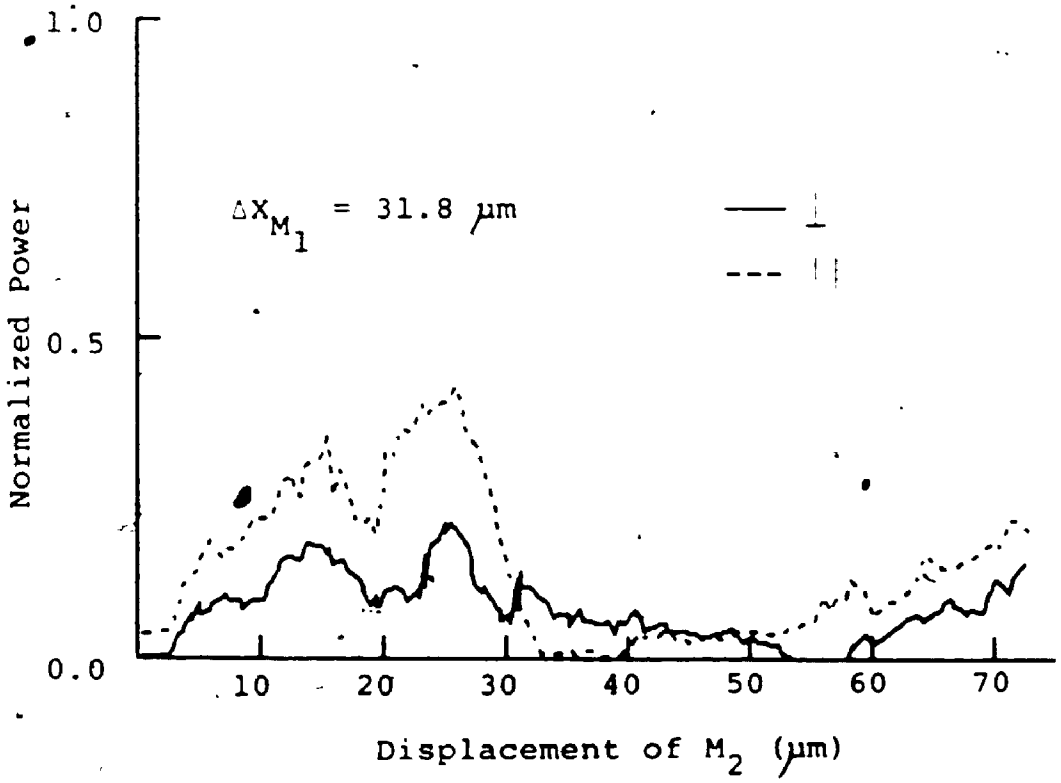
1.0
0.5
0.0
Normalized Power
ΔX_{M_1} = 31.8 μm
⊥
||
10
20
30
40
50
60
70
Displacement of M_2 (μm)

(f)

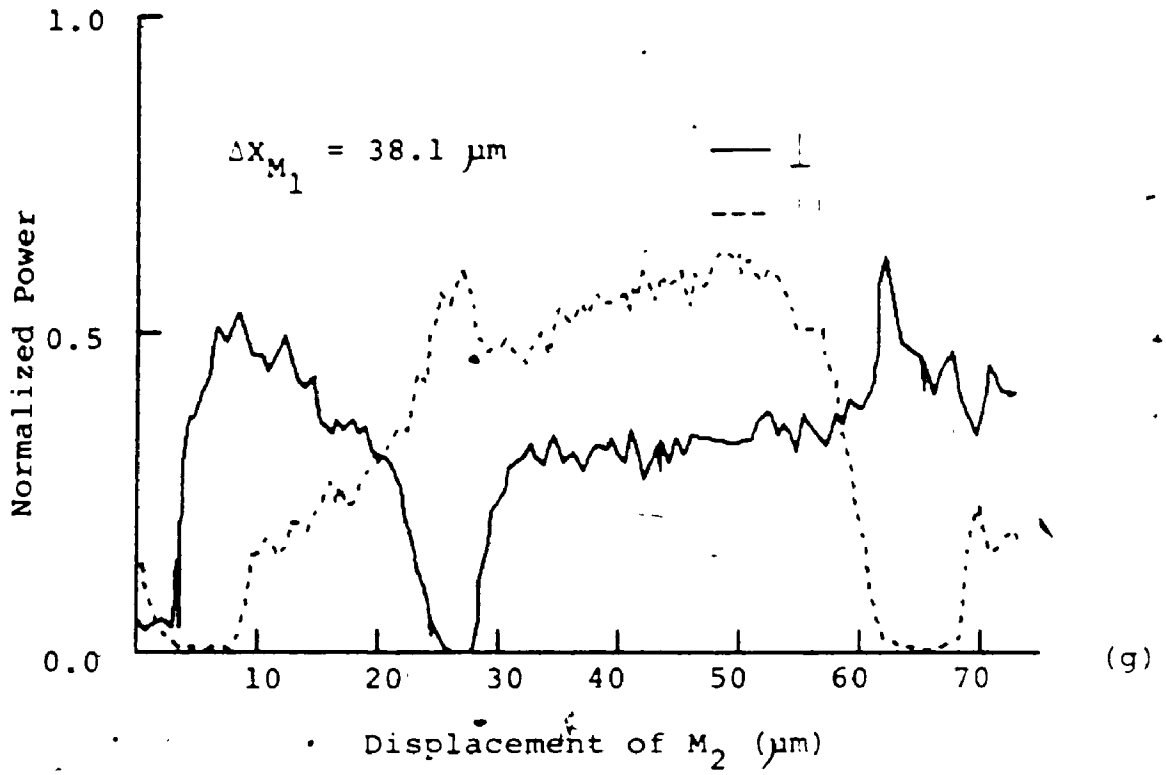
1.0
0.5
0.0
Normalized Power
ΔX_{M_1} = 38.1 μm
⊥
||
10
20
30
40
50
60
70
Displacement of M_2 (μm)

(g)

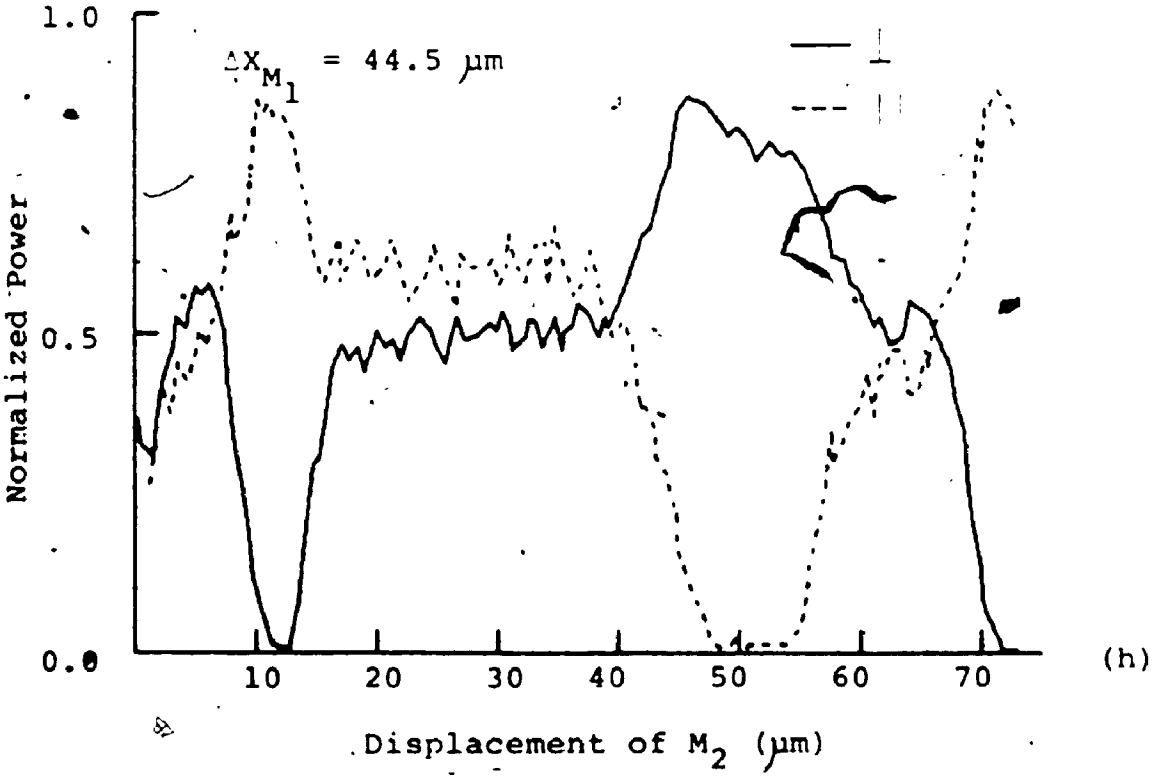
1.0
0.5
0.0
Normalized Power
ΔX_{M_1} = 44.5 μm
⊥
||
10
20
30
40
50
60
70
Displacement of M_2 (μm)

(h)

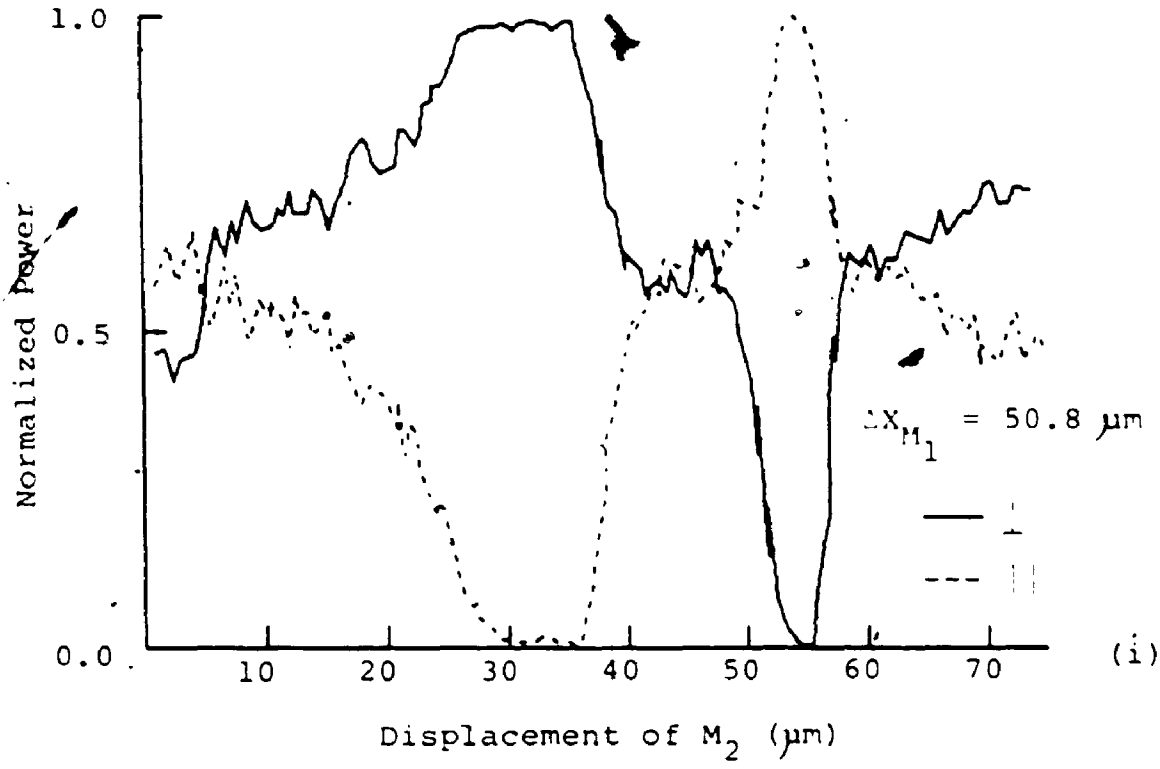
1.0
0.5
0.0
Normalized Power
10
20
30
40
50
60
70
ΔX_{M_1} = 50.8 μm
⊥
∥
Displacement of M_2 (μm)

(i)

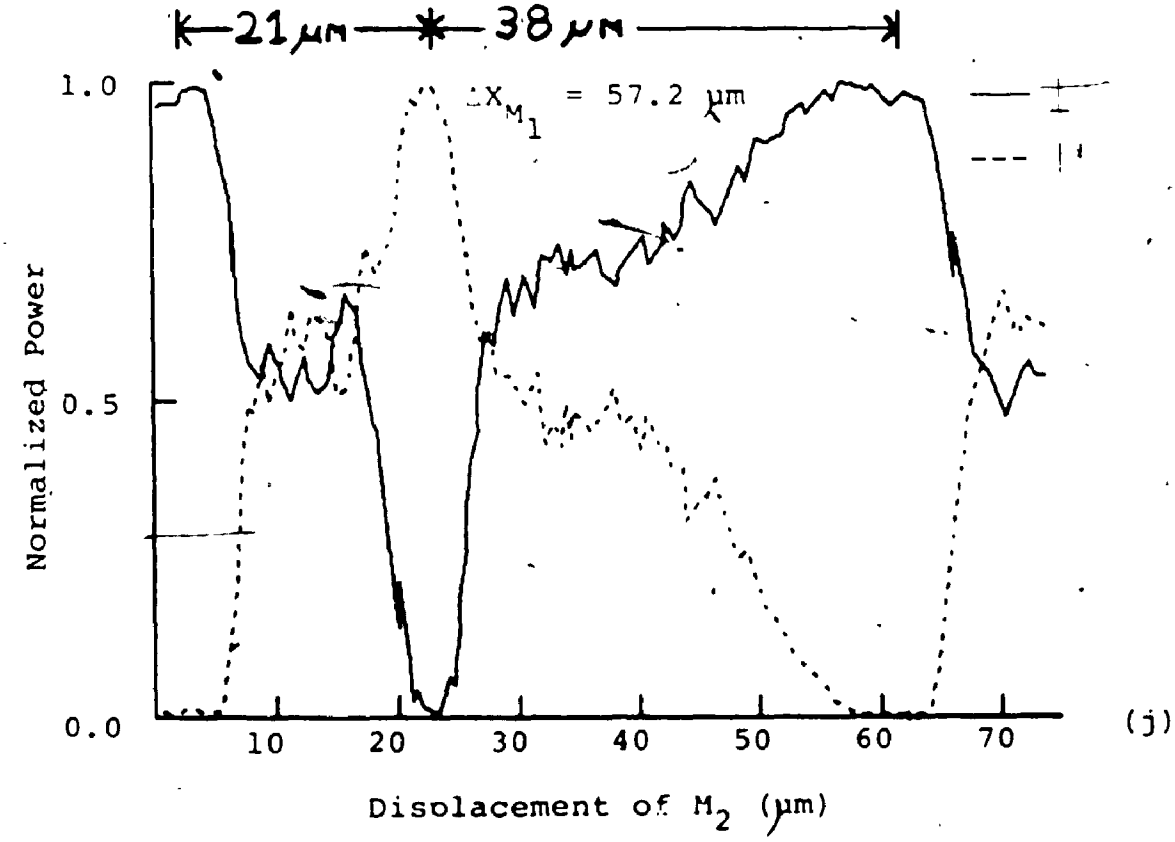
21μm
38μm
1.0
0.5
0.0
Normalized Power
ΔX_{M_1} = 57.2 μm
⊥
∥
10
20
30
40
50
60
70
Disolacement of M_2 (μm)

(j)

detector element did not have a window.

Figures 5.1 and 5.2 are sample results of experiments done with the MGM resonator at 118.6 micrometer. (Figure 5.1 is the experimental result where the secondary mirror, M2, was moved in steps, and figure 5.2 is the result where the primary mirror, M1, was moved in steps.) Both figures show the signal of each polarization normalized to their respective maximum signal. The $\perp$ symbol in the figures refers to radiation perpendicularly polarized relative the lines of the principal grating, and the $\parallel$ signal refers to parallel polarized radiation. The peak power of the perpendicular radiation from the MGM laser was about the same as the peak power from the simple mirror-grating laser.

As reported by Sarjeant and Brannen (1970), the results presented in figures 5.1 and 5.2 confirm that the MGM resonator can produce laser radiation polarized either perpendicular or parallel or both to the principal grating ruling, and that the output depended on the position of the secondary mirror.

In figure 5.1, the powers of both polarization modes were modulated nearly in phase with the translation of the primary mirror, M_1. However, the value of the peak power of the two modes was determined by the position of the secondary mirror. There appears to be at most a 4 micrometer offset

between the modulation of the two modes and there was no apparent change in this offset with the different position of the secondary mirror.

In figure 5.2, the competition of the two polarization modes can be seen down to the small scale. The figure demonstrates, like figure 5.1, the positional influence of the secondary mirror on the power of the two modes. For both polarization modes, at different narrow range positions of the secondary mirror, the power of one of the modes peaked, such that its power completely dominated and robbed the other mode of laser gain, and suppressing it completely (see figures 5.2 h, i, j). The power peaking of both modes are $\lambda/2$ periodic (period = 118.6/2 micrometers), and, as mentioned before, occur at different relative position of the secondary mirror. The modes peaked when the resonant frequency of the secondary cavity, formed between the primary grating and the secondary mirror, equaled the resonant frequency of the primary grating (see chapter 2). This positional difference will be discussed below.

The figure 5.2 also shows that the peak and intermediate powers of the two modes were modulated by the translation of the primary mirror. Again it can be seen that the power modulation of the two modes are nearly in phase.

As shown in figure 5.2, the secondary cavity frequency

for each mode equals the primary cavity frequency at two different positions of the secondary mirror. From measurements of several experiments similar to the one presented in figure 5.2, the peak power positional difference of the secondary mirror was 21 $\pm$ 2 micrometers or 38 $\pm$ 2 micrometers depending on the direction of measurement (see figure 5.2j) (the direction of the measurement will be discussed below). The frequency of the two modes in the main cavity can be assumed to be the same or nearly the same so that the optical planes of reflection of the primary grating for the two modes must not be coincident.

To calculate the optical plane difference for the two polarizations, the model of grating reflection described in chapter 2 will be used. It will be assumed that the frequency and phase of the two polarizations in the main cavity are the same. The path difference, ΔL, from reflection from the grating is equal to the peak power position difference of the secondary mirror (see figure 5.2 j). From the model, the parallel optical plane is in front of the perpendicular plane, so that when the secondary mirror travels toward the primary grating the peak power path difference must be measured from the parallel peak power position to the perpendicular peak power position. For experiments where the secondary mirror travelled away from the primary grating, the measurement must be done in opposite fashion. From this prescribed way of measuring , the path difference equals 38 $\pm$ 2

In subsequent experiments, the single mode laser power of the 47.47 and 47.70 micrometer lines as secondary lines in the MGG laser was compared when the radiation was parallel or perpendicular to the primary grating ruling. The primary grating was the 30 micrometer blazed grating, and the secondary grating was the 47 micrometer blazed grating, both described in previous sections. The experiment was done by first measuring the laser power with the radiation perpendicular to the lines of the primary grating (the lines of the two gratings in parallel), and then parallel to the lines. The procedure was then repeated again.

For the 47.47 micrometer line, the ratio of parallel to perpendicular polarized power (relative to the primary grating lines) was 2.4 ± 0.1, while for the 47.70 micrometer line the ratio was 4.1 ± 0.1.

These results demonstrate that the primary grating is more reflective for radiation polarized parallel to its ruling lines than for perpendicularly polarized radiation. Thus the best design of MGG resonator for maximum power for non interacting two-line operation would be with the grating lines perpendicular to each other. For the cases of competing or cascading lines, coupling effects have to be taken into account before deciding on the optimum relative orientation of the laser:

measured the coefficient to be equal to 0.21 with a 26.75 degrees blazed grating (Hutchinson, 1981b). Both coefficient values were with wavelengths more than twice the grating rule spacing, and the radiation was incident normal to the grating (see chapter 2). The present measured coefficient value of 0.32 ± 0.02 is in good agreement with both the theoretical and experimental values. From Hutchinson's theoretical calculations, the coefficient is expected to decrease to 0.16 for wavelengths much longer than the ruling spacing. The present measured coefficient value which was measured with a wavelength shorter than the grating line spacing may be continuing the theoretical established trend for shorter wavelengths.

5.3 CONCLUSION

It has been shown that the laser polarization can be controlled with an MGM laser resonator. Also, the polarization control is a function of the secondary resonator length and the overall power is a function of the primary resonator length. Thus a laser could be designed where lasing frequency could be controlled by maximizing the overall power, and the relative polarization power could be controlled with the translation to the secondary mirror. The travel of the secondary mirror for polarization switching is small compared to the lasing line half-wavelength.

From the experimental results, the polarization optical

plane difference was measured. From the groove depth of the grating the optical plane difference coefficient was calculated. The coefficient was found to be in good agreement with both theoretical and experimental values, taking into account the differences of basic parameters, showing that the optical plane difference scales with the groove depth of the grating.

Experiments could validate the optical plane model of the grating and compare it with the results found at 118.6 micrometers, to find out if the optical plane difference varies with reflection angle or not. The experiments could use the three strong water vapour lines, the 26.6, 27.97 and 33 micrometer lines, combined with the 30 micrometer blazed grating. All three lines can lase with the grating, and their Littrow angles are 23.5 degrees for the 26.6 micrometer, 24.8 degrees for 27.97 micrometer, and 29.7 degrees for the 33.0 micrometer, giving a good variation of angles for the experiment with the same grating. Since the blaze angle of the 118 micrometer grating is nearly the same as the 30 micrometer grating the results from these experiments would test the scaling of the grating parameters. The experiment would have to be done with a shorter laser and maybe higher pressures to avoid the problem of two longitudinal modes within the gain curve. For these wavelengths a smaller diameter laser tube would also be desirable (25 to 50 millimeters I.D) to increase the gain.

CHAPTER 6

MIRROR-GRATING-GRATING EXPERIMENTS AND RESULTS

The mirror-grating-grating (MGG) resonator allows two far-infrared lines to lase simultaneously, co-axially and with control over the relative polarization of the two lines. Other coupling measurements in the far-infrared have had to be done with two resonators set in an 'X' configuration within the laser tube (Jeffers, 1968). This configuration does not allow the efficient use of the lasing medium for interaction between the two lines. Also, because of awkward optical set up, the laser tube cannot be made smaller without making the optical resonator longer so that both resonator beams will fit within the laser tube. The interaction between two lines in an MGG resonator is along the whole lasing medium length allowing much greater overlap of the medium for the two lines and is in the centre of the optical axis where usually there is the maximum gain and saturation. The optical set-up is relatively simple and no limitation is placed on the length to diameter ratio of the laser tube.

As in the MGM resonator case, Sarjeant and Brannen (1970) demonstrated that the MGG resonator would allow lasing

on two lines simultaneously in a controlled manner.

This chapter describes the experimental methods developed and used with the MGG resonator laser, the optical properties found, and experimental results of simultaneous lasing for several pairs of interacting water vapour laser lines.

6.1 MGG EXPERIMENTAL METHODOLOGY

The alignment procedure for the MGG resonator was similar to that of the MGM resonator. The only difference is that the lasing of the short wavelength (lasing from the primary grating) was suppressed while the final alignment of the secondary grating for the long wavelength was being done. The short wavelength was suppressed by de-tuning the primary grating from the Littrow configuration.

The following methodology was followed for coupled line interaction experiments. The short wavelength was set for maximum power by adjusting the settings of the primary grating, G_1, and principal mirror, M_1: the absorber was placed within the secondary cavity to suppress the long line from lasing. The absorber was then removed and the settings of the second grating, G_2, were adjusted for maximum power. This constituted the laser's interaction configuration. The single line power of short wavelength was measured several times while the laser was in the interaction configuration by

placing the absorber in and out of the secondary cavity. To measure the single line power of the long wavelength, the primary grating was rotated slightly about the vertical axis so that the short wavelength would not lase, and then the secondary grating was readjusted for maximum lasing power.

Usually, in the first part of the experiment the polarization of the two laser lines were aligned (the lines of the two gratings were parallel). To measure the interaction of the two lines with the polarization perpendicular to each other, the secondary grating was rotated 90 degrees about the optical axis (the grating surface facing up), and the above interaction procedure repeated. Depending on the experiment, up to four sets of measurements were taken, two with the grating rulings in line, and two with them perpendicular.

In a preliminary experiment, the 27.97 and 118.6 lines were made to lase simultaneously. To reduce the losses for the 118.6 line, the laser iris had to be opened fully (60 millimeters). Because of the high gain of the 27.97 line and the large laser aperture, the 27.97 transverse modes lased and could not be suppressed without the 118.6 micrometer line also being inhibited. The 27.97 micrometer output power fluctuated severely, and would have undermined any attempted correlation experiments. The design of the MGG resonator does not lead to a simple solution to this problem. As the

difference in wavelength of the two lines used with the MGG resonator lessen, the transverse mode excitation problem reduces. For the lines studied, the difference in wavelength and power of the two lines were such that the iris could be closed enough so that transverse modes of the short wavelength lines were not excited.

6:2 MGG OPTICAL PROPERTIES

The primary grating in the MGG resonator acts as a mirror for the second longer wavelength. However, unlike a plane mirror, the primary grating reflection properties depend on the polarization of the incident radiation. Some of the optical reflection properties of primary gratings were investigated experimentally.

In experiments where the primary grating was used solely as a reflection element, certain weaker water vapour line used as the secondary wavelength of the MGG laser could not lase, or lased with reduced power. This result is attributed to the extra reflection loss from the primary grating. For example the 49.1 micrometer line could lase in an MG laser resonator, but could not lase as the secondary wavelength off the MGG laser. The power of the 118.6 micrometer line as the second line was greatly reduced as compared with the power output from the MG laser. In both experiments, the ruling of the two gratings were parallel to each other.

In subsequent experiments, the single mode laser power of the 47.47 and 47.70 micrometer lines as secondary lines in the MGG laser was compared when the radiation was parallel or perpendicular to the primary grating ruling. The primary grating was the 30 micrometer blazed grating, and the secondary grating was the 47 micrometer blazed grating, both described in previous sections. The experiment was done by first measuring the laser power with the radiation perpendicular to the lines of the primary grating (the lines of the two gratings in parallel), and then parallel to the lines. The procedure was then repeated again.

For the 47.47 micrometer line, the ratio of parallel to perpendicular polarized power (relative to the primary grating lines) was 2.4 ± 0.1, while for the 47.70 micrometer line the ratio was 4.1 ± 0.1.

These results demonstrate that the primary grating is more reflective for radiation polarized parallel to its ruling lines than for perpendicularly polarized radiation. Thus the best design of MGG resonator for maximum power for non interacting two-line operation would be with the grating lines perpendicular to each other. For the cases of competing or cascading lines, coupling effects have to be taken into account before deciding on the optimum relative orientation of the laser.

From these experimental results, the ratio of the 47.47 to 47.70 micrometer single line power in the MGG resonator could be also calculated under similar lasing conditions. When the polarization of the two lines was perpendicular to the primary grating, the power ratio of the 47.47 to 47.70 micrometer lines was 0.41 $\pm$ 0.01 and when the polarization of the lines was parallel, the ratio was 0.24 $\pm$ 0.01.

Another reflection property was found during the preliminary MGG experiments. In these experiments, the secondary grating was rotated about the optical axis in steps of 22.5 degrees, starting at 0 degrees (the grating lines parallel to each other) to 90 degrees. When polarization measurements of the secondary line were made, it was found that the polarization of the radiation was perpendicular to the primary grating rulings when the secondary grating was set at 0 and 22.5 degrees, and parallel when the secondary grating was set at 67.5 and 90 degrees. When the secondary grating was set at 45 degrees, both polarization modes were lasing. These results were found for both the 47.47 and 47.70 micrometer lines. Figures 6.1a to 6.1c show polarization measurements of the 47.47 micrometer line with the grating at 0, 90 and 45 degrees. The overall lasing power decreased with the rotation of the grating to a minimum at 45 degrees.

When the secondary grating was set at 45 degrees, the relative power of the two polarization modes was not consis-

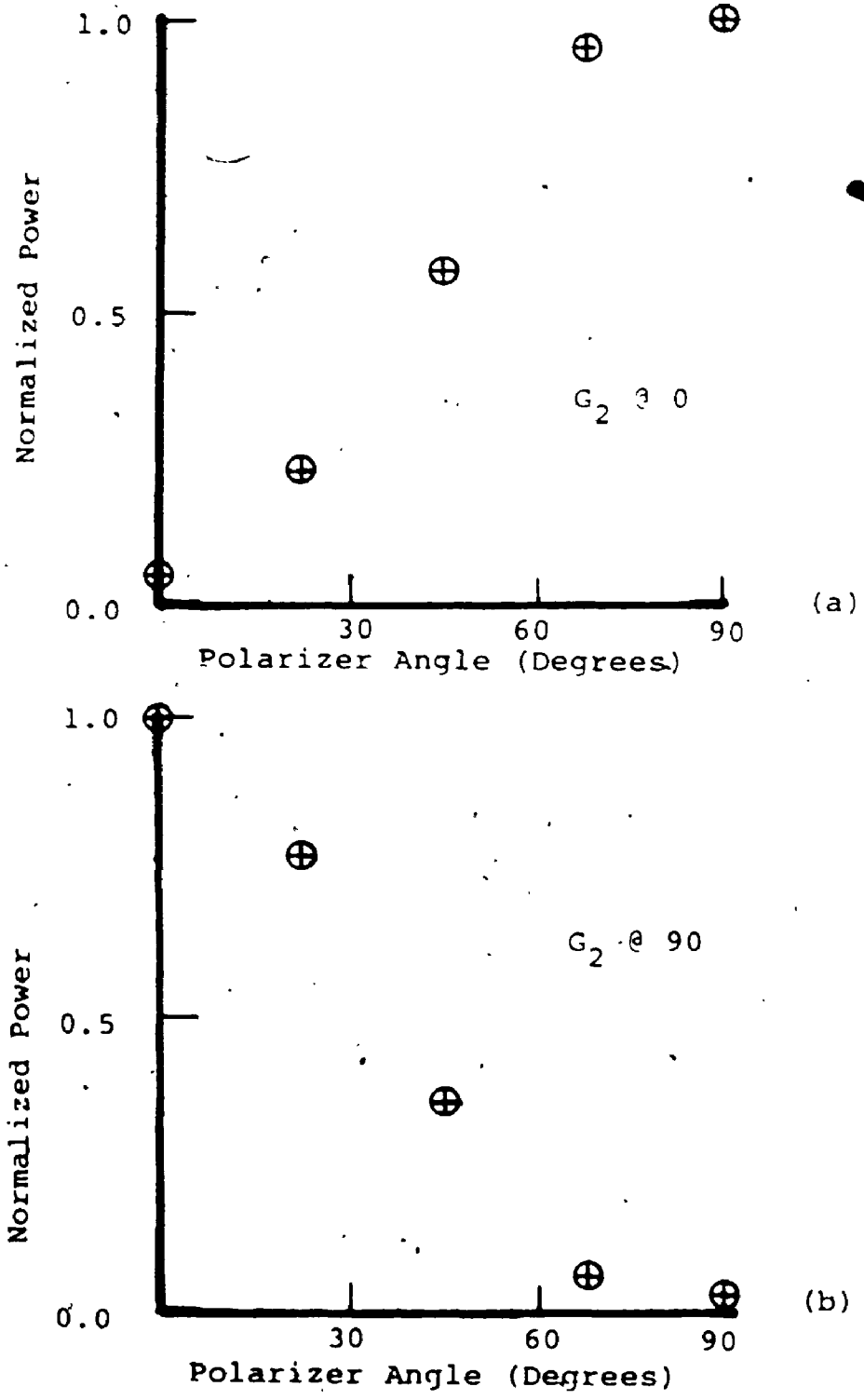

Figure 6-1
Normalized Power versus Polarizer Angle
for 0, 90, 45 Degrees Relative Angle
Between the Primary and Secondary Grating

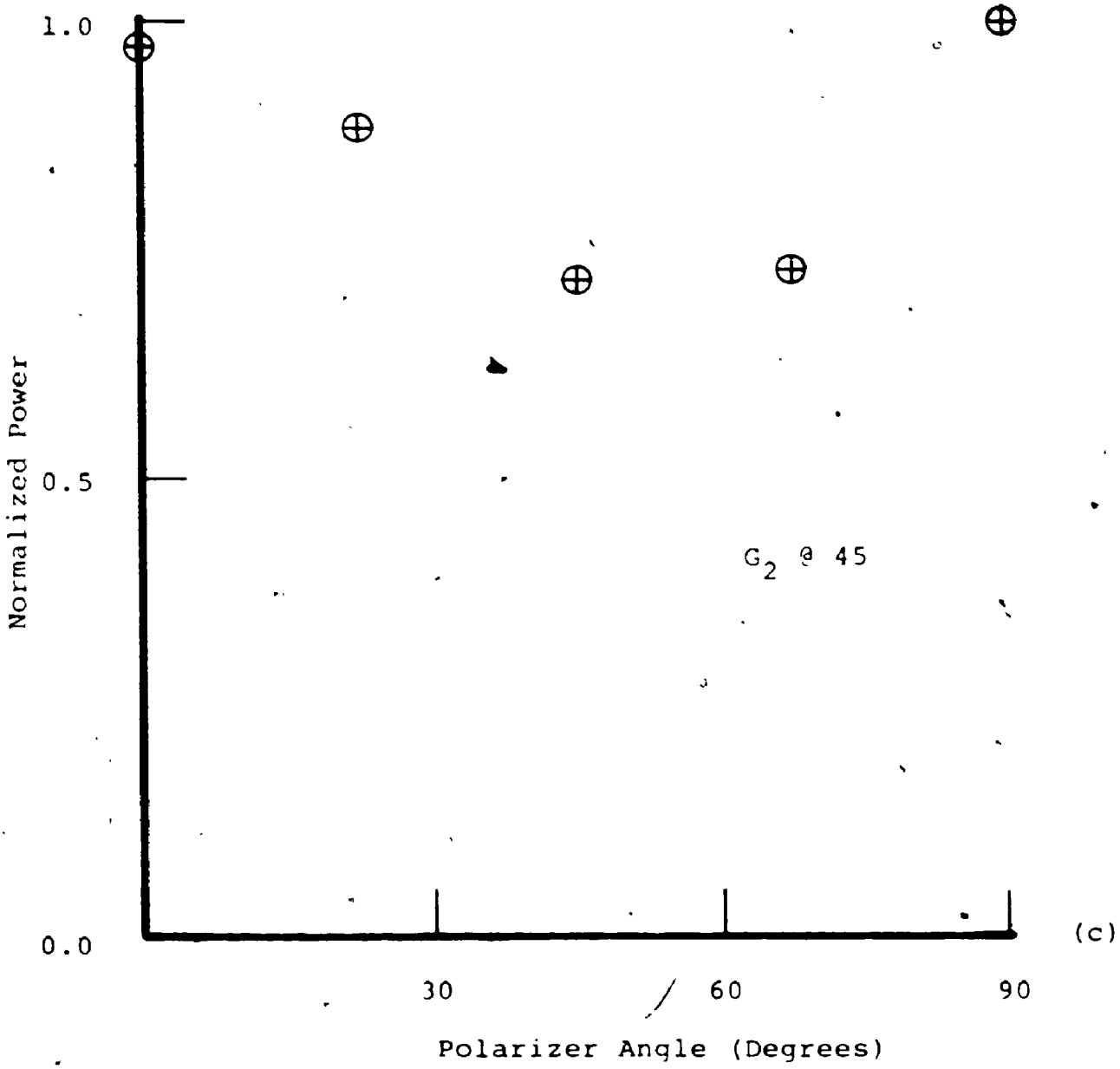
1.0
0.5
0.0
Normalized Power
G_2 @ 45
(c)
30
60
90
Polarizer Angle (Degrees)

tent from trial to trial. This may be due to the relative position of the secondary grating or the critical dependence on the relative grating angle. From observation of the lasing signal on a dual channel oscilloscope (chopping mode), no alternation of power between the two polarization modes from pulse to pulse was observed.

These results are consistent with the grating model described before. When the secondary grating ruling was either parallel or perpendicular to the primary grating, the radiation reflected off the primary grating like a mirror. As the secondary grating was rotated about the optical axis, the linearly polarized lasing radiation from the secondary grating was split on the primary grating into two perpendicular polarizations (perpendicular and parallel to primary grating rulings), because of the polarization optical plane difference of the primary grating. The two polarization modes have an overall different optical path length and so are resonant at sightly different frequencies. When the secondary grating was set at 22.5 and 67:5 degrees about the optical axis, the losses were too great to sustain the parallel and perpendicular polarization modes, respectively, so that the laser radiation was linearly polarized perpendicularly and parallel, respectively, but at lower power. When the secondary grating was set at 45 degrees, the secondary radiation is more evenly split by the primary grating, and thus both polarization modes of the secondary line could lase.

It would be interesting to measure the optical plane difference of the primary grating at the wavelength longer than the critical wavelength. One way, other than the heterodyne method described in section 2.4, would be to use an MGM resonator set so that the short wavelength would not lase from the secondary mirror and the long wavelength would lase. Simultaneous measurement of the two polarization modes of the longer wavelength could then be taken. Assuming that the results would be similar to those found when the lasing wavelength was shorter than the critical wavelength of the grating, the same type of analysis as described in chapter 5 could be used to calculate the optical plane difference of the primary grating.

6.3 TWO-LINE INTERACTION RESULTS

As mentioned before, water vapour is a good lasing medium to study interacting lasing lines. Water vapour has many lines that are in cascade or in competition. Unfortunately many of the lines have gain too small to be used in experiments. The choice is then reduced to lines that have good output power and share an energy level. Another practical constraint is the available grating for the MGG resonator.

Four lines were finally chosen for detailed investigation; 26.6, 27.97, 47.47 and 47.70 micrometer lines. These

(Benedict et al., 1969), common energy levels, and good power output. Figure 6.2 shows schematically the vibrational-rotational energy levels (from Benedict et al., 1969) of the four chosen lines as well as other lines used with both the MGM and MGG laser.

Unfortunately all the interacting lines used in the experiments are competitive. No suitable lines were available for a cascade interaction experiment either because the lines are too weak, for example the 49 and 120 micrometer lines, or because no suitable grating was readily available for one of the cascade transitions.

The 26.6 and 27.97 micrometer lines lased with the 30 micrometer blazed grating as the primary grating. The 47.47 and 47.70 micrometer lines lased with the 47 micrometer blazed grating as the secondary grating.

Because the 47.47 and 47.70 micrometer lines are so close, special care had to be taken to ensure that only one line was lasing at a time. This was accomplished by closing the iris down to about 25 mm. The long length of the laser also helped separate the two lines. The small aperture reduced the power of both 47 micrometer lines but the power levels were sufficient to carry out the experiments.

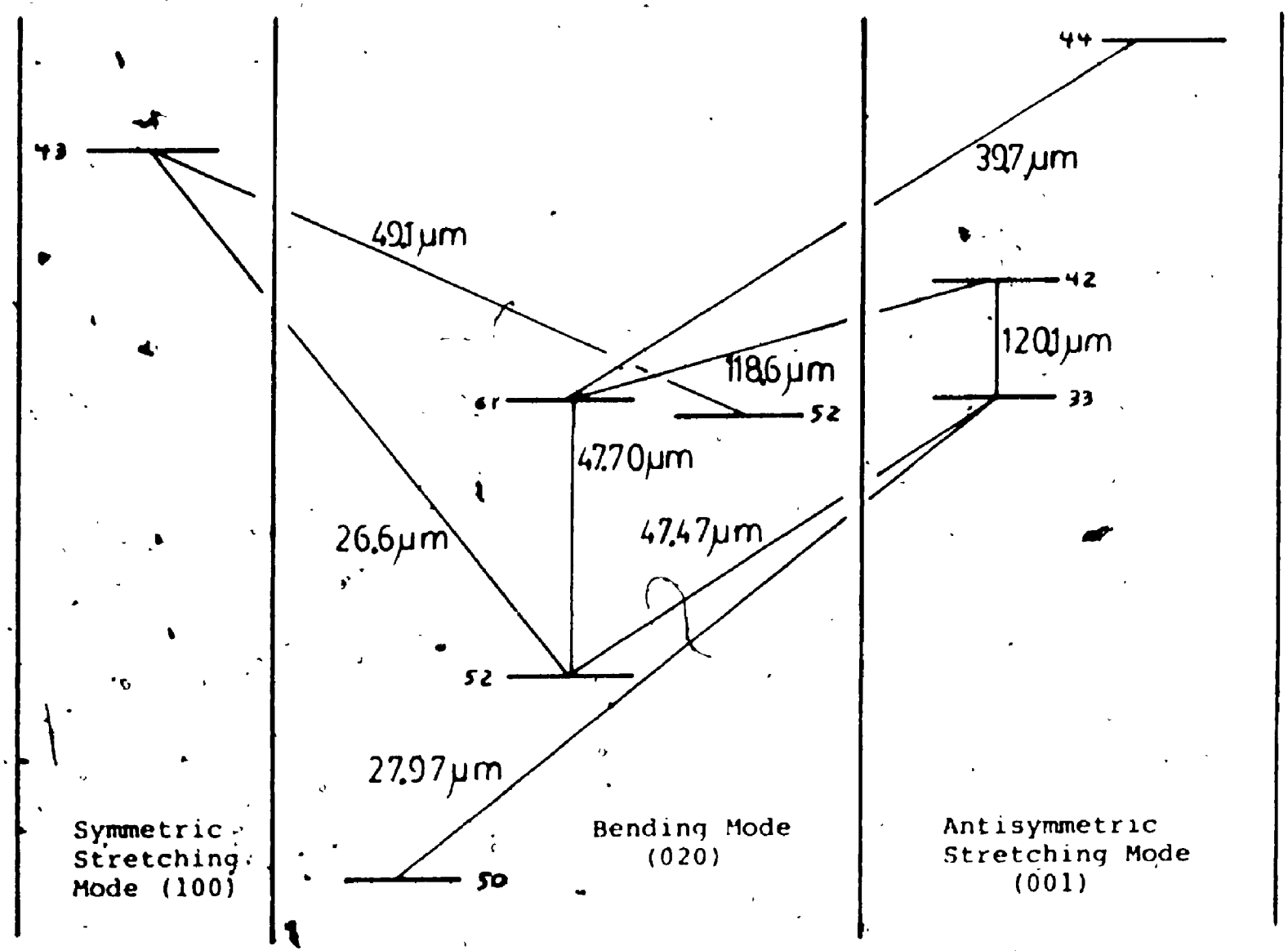

Figure 6-2
Water Vapour Laser Transitions

6.3.1 INTERACTION RESULTS FOR THE 26.6 AND 47.70 MICROMETER LINES -

The experimental results for the 26.6 and 47.70 micrometer lines were the most satisfying of the four interaction experiments. From the results of this pair of lines could the coupling constants be calculated. When the interaction experiments were done with the three other pairs of lines, the lasing power of the short wavelengths did not change sufficiently (relative to the noise) to allow the coupling constant to be calculated with the method described in Chapter 3. The power of the long wavelength lines did change appreciably demonstrating that the lines were coupled, and the coupling depended on the polarization allowing estimates of J values involved in the two transitions (see the following sections for more detail).

Typically in the two-line experiment the, power of the 26.6 micrometer line would decrease by about 21 percent, and the 47.70 micrometer line by 23 percent when the polarizations modes of the two lines were parallel. When the polarization of the two lines were perpendicular to each other, the power of the 26.6 micrometer line would decrease by about 36 percent, and the 47.70 micrometer line by about 56 percent. (For all the percentages above and following, the single mode power of the line is used as a standard in the calculation.)

The parallel polarization coupling constant was calculated from the experimental results to be 0.18 ± 0.04, and for perpendicular polarization to be 0.45 ± 0.06. The ratio of the parallel to perpendicular coupling constant was 0.40 ± 0.14.

The experimental coupling constant is a measure of the magnetic coupling constant, dependent on the relative polarization of the lines, multiplied by the non-degenerate coupling constant. The theoretical expressions for the coupling constants contain terms involving the electric dipole moments of the transitions, decay constants, and pumping rates. These are generally not known so that the experimentally obtained values can not be compared directly with the theoretical values. However, given the angular momenta of the transition levels and the polarization type of the two interacting lines, the contribution of the magnetic sub-levels to the coupling constant can be calculated. Thus the ratio of the experimentally measured parallel to perpendicular coupling constants is the ratio of only the magnetic sub-level parts of the coupling constants, and can be compared to the theoretical calculations.

According to Benedict et al. (1969), the 26.6 and 47.70 transitions have a common lower level of $J = 6$. For the 26.6 micrometer line $\Delta J = 1$, and for the 47.70 micrometer line, $\Delta J = 0$.

According to Melekhin and Melekhina, 1973, for two transitions whose radiations are linearly polarized and $\Delta J_1 = 0$, $\Delta J_2 = 1$, the magnetic coupling constant can be calculated from

$$C' = \frac{J(J+2)^2(2J+3)}{(3J^2+3J-1)(4J^2+8J+5)} \qquad \text{(parallel polarization)}$$

and

$$C' = \frac{J(2J+3)(4J+3)^2}{4(3J^2+3J-1)(4J^2+8J+5)} \qquad \text{(perpendicular polarization)}$$

With the given values for the 26.6 and 47.70 micrometer transitions, the calculated value of the parallel magnetic coupling constant is 0.234 and for the perpendicular is 0.666. The ratio of the parallel to perpendicular magnetic coupling constant is equal to 0.351 in reasonable agreement with the experimental ratio (0.40 ± 0.14).

6.3.4 INTERACTION RESULTS FOR THE 26.6 AND 47.47 MICROMETER LINES

The least amount of interaction was found with this pair of lines. When the two lines lased simultaneously, the 26.6 micrometer line power did not change perceptibly for either relative linear polarization. The 47.47 micrometer line power reduced only about 6 percent when the polarization

of the lines were parallel, and 11 percent when they were perpendicular. The experimental conditions were similar to the experiments with the 26.6 and 47.70 micrometer line. The power of the 26.6 micrometer line was almost the same in both experiments.

The results indicate a slight increase in coupling when the line polarizations are perpendicular to each other as compared to when they are parallel. The results indicate that the J of the two transitions are not equal. The result are consistent with the transition scheme of the 26.6 and 47.47 micrometer line presented by Benedict et al.; $\Delta J = 1$ for the 26.6 micrometer line, $\Delta J = 0$ for the 47.47 micrometer line, and the $J = 6$ for the common lower energy level.

6.3.3 INTERACTION RESULTS FOR THE 27.97 AND 47.70 MICROMETER LINES

According to the transition scheme of Benedict et al. (1969), the 27.97 and 47.70 micrometer transition do not share directly an energy level. However, the energy levels are quasi-degenerate and their wavefunctions mix. The mixing of the wavefunction increases the probability of a transition from the symmetric vibrational stretching mode to the bending mode (like for the 27.97 micrometer transition). The mixing also provides a coupling mechanism between the two transitions. The wavefunction mixing of quasi-degenerate energy levels between the stretching modes and the bending modes

plays a major role in the lasing mechanism of water vapour (see Benedict et. al., 1969).

When the interaction experiment was performed with the 27.97 and 47.70 micrometer lines, the power of the 27.97 micrometer line did not change, while that of the 47.70 micrometer line was reduced to practically zero for either relative line polarizations. From the results, it is obvious that the two lines are very strongly coupled for either polarization. The interesting aspect of these results is the complete suppression of the 47.70 micrometer line.

6.3.4 INTERACTION RESULTS FOR THE 27.97 AND 47.47 MICROMETER LINES

When the 27.97 and 47.47 micrometer line were made to lase simultaneously, the 27.97 micrometer line power did not change to any noticeable degree, similarly to the 27.97 and 47.70 micrometer lines experiments. The 47.47 micrometer line power, when interacting with the 27.97 micrometer line, was reduced by about 96 percent when the two laser lines were polarized parallel to each other, and 48 percent when the two were perpendicularly polarized to each other. The 27.97 micrometer line power was about the same as in the 27.97 and 47.70 micrometer interaction experiment.

According to the Benedict et al. (1969), the 27.97 and 47.47 micrometer lines share a common upper energy level,

J = 6. According to the transition scheme, for the 27.97 micrometer line, $\Delta J = -1$, relative to the common upper level, and for the 47.47 micrometer line, $\Delta J = 0$. From the magnetic coupling model, described in chapter 2, the two transitions should couple more when the relative polarization of the two lines are perpendicular to each other. The experimental coupling results are just the opposite. Outside of an incorrect rotational assignment, there does not seem to be any straightforward explanation for these results.

6.4 CONCLUSION

It has been shown that the MGG resonator can be used to investigate the coupling of two laser lines that share a common transition energy level. It has also been shown that the coupling depends on the relative polarization of the two lines as predicted by the sub-magnetic coupling model.

Four pairs of water vapour laser lines were investigated. The ratio of the theoretical relative polarization coupling constant to the ratio of the experimental constants were in good agreement for the 26.6 and 47.70 micrometer lines with the given transition assignment. The coupling between the 26.6 and 47.47 micrometer lines was very small but consistent with the given transition assignment. The 47.70 micrometer line was completely suppressed when the 27.97 micrometer line lased in either relative polarization. The 27.97 and 47.47 micrometer lines showed the strongest

coupling when the two lines were parallel to each other, opposite to what was expected from the given energy level assignments. For the 26.6-47.47 micrometer, the 27.97-47.70 micrometer and the 27.97-47.47 micrometer interaction experiments, the power of the short wavelengths did not change noticeably with the experimental noise level to be able to calculate coupling constants.

Several polarization reflection properties of the primary grating for radiation of wavelengths longer than the critical wavelength were investigated by using the MGG laser in single mode configuration and lasing from the secondary grating. The reflection coefficient of the primary grating for radiation polarized parallel to the grating lines was found to be greater than for perpendicularly polarized radiation. This is an important feature for the design of a MGG laser when maximum power of two non-interacting lines is wanted.

The polarization of the second line in the MGG compound resonator was found to be parallel or perpendicular (or both in a special case) to the primary grating lines as the secondary grating was rotated about the optical axis. This feature is consistent with the grating model of a difference in position of optical plane of reflection for parallel and perpendicular polarized radiation.

CHAPTER 7

CONCLUSIONS

The interaction of several coupled laser lines was investigated with the use of a compound MGM laser resonator. The MGM resonator allows two lines to lase simultaneously and co-axially with control of the relative polarization of the two lines. From the nature of the MGM resonator the polarization of the two lines can only be parallel or perpendicular to each other.

Four pairs of coupled water vapour lines all in competition were investigated; the 26.6 and 47.70 micrometer lines, the 26.6 and 47.47 micrometer lines, the 27.97 and 47.70 micrometer lines, and the 27.97 and 47.47 micrometer lines. Because all the pairs of transitions had a common upper or lower energy level, the coupling between them was competitive so that the power of one or of the other or both lines was reduced when the two lased simultaneously. The power suppression of three of the four pairs of lines showed dependence on the relative polarization of the two lines: the 47.70 micrometer line was completely suppressed whenever the

27.97 line lased simultaneously with either relative polarization.

From the interaction results of the 26.6 and 47.70 micrometer lines two coupling constants were calculated: one when the polarization of the two lines were parallel, $C = 0.18 \pm 0.04$, and another when they were perpendicular $C = 0.45 \pm 0.06$.

The coupling constant is not only a function of such factors as dipole moments of the transitions, pumping and decay rates of the energy levels but also on how much the two transitions compete for the magnetic sub-levels population. The magnetic sub-level competition depends on the relative polarization of the two transitions, and on values and change in values of the angular momentum of the transitions. The ratio of the coupling constant is a measure of difference in coupling of the two lines at the sub-magnetic level, the other coupling factors do not depend on the relative polarization of the lines. The ratio of the parallel to perpendicular coupling constants for the 26.6, 47.70 micrometer lines is 0.40 ± 0.14 and compares well to the theoretical predicted value of 0.35.

Because the power of the 26.6 and 27.97 micrometer lines did not change noticeably compared to the experimental noise level for the three other pairs of lines (26.6-47.47, 27.97-

47.47 and 27.97-47.70 micrometer lines) when made to lase simultaneously, no other coupling constant could be calculated. However the power suppression of the longer wavelengths of the 26.6-47.47 and 27.97-47.70 micrometer lines did depend on the relative polarization of the two lines: as mentioned above, the 47.47 micrometer line was completely suppressed by the 27.97 micrometer line with either relative polarization.

When the polarization of the 26.6 and the 47.47 micrometer lines were perpendicular to each other, the 47.47 micrometer line was more suppressed than when the polarizations were parallel, as predicted theoretically with the given energy assignments. For the 27.97 and 47.47 micrometer lines, the suppression of the 47.47 micrometer line was greatest when the polarization of the two lines were parallel to each other, and less when they were perpendicular to each other. This last result is the opposite of what was expected with the given levels assignments.

The major limitation for the coupling measurement was signal noise due to the variation of power from pulse to pulse. For certain coupled lines, this problem could be circumvented by performing the experiments with the laser in CW mode if the second line has enough gain to overcome the extra reflection loss off the primary grating. However many coupled laser lines cannot lase CW, and so the only other alternative is to reduce the pulse to pulse variation of

power, not an easily solved problem in a high current gas discharge laser.

The features of mirror-grating-mirror resonator were also investigated. This laser resonator allows the control on the polarization of the laser radiation with the position of the secondary mirror. Simultaneous measurements of both polarization modes were taken as either the secondary or primary mirrors were translated. The radiation could be either polarized perpendicular or parallel or both to the lines of the principal grating.

A model was developed to explain the interaction between the secondary mirror and the primary grating of the resonator that gives the above results. Essentially the secondary mirror forms a coupled cavity. However, the optical paths for the two polarization modes are slightly different because of the reflection properties of the grating: the optical planes of reflection for the grating are at different positions for the two polarizations of radiation. The resulting difference in optical path length for the two polarizations (parallel and perpendicular) means that the secondary cavity will come into resonance with the primary cavity for one of the polarization modes (making the radiation singly polarized) at a different position of the secondary mirror than for the other polarization mode.

From the experimental results of the mirror-grating-mirror resonator the optical plane separation for a 30 micrometer grating(d = 1/[6666] meters per line, blaze angle = 23.5 degrees) was 38 $\pm$ 2 micrometers. An optical plane coefficient, γ, is defined as the ratio of the optical plane separation to the groove depth of the grating. The coefficient is defined because theoretical models of the optical plane predict that the difference should scale with the groove depth of the grating. The optical plane difference for the 30 micrometer grating is 0.32 $\pm$ 0.02, in fairly good agreement with the theoretically calculated value of 0.21.

APPENDIX A

SEMI-CLASSICAL THEORY OF COUPLED TRANSITIONS

In this appendix, the semi-classical theory of the coupling of two transitions that share a common energy level will be outlined. The semi-classical approach to laser interaction treats the electromagnetic radiation as a classical wave interacting with molecules (atoms) that obey quantum mechanics (Sargent et al., 1974). There are several treatments of coupled transitions that follow the semiclassical approach (Haken et al., 1965, Najmabadi et al., 1975, Paxton and Milonni, 1980, Agrawal, 1984), and also a fully quantum mechanical derivation of coupled laser transitions (Singh and Zubairy, 1980, 1981). The theoretical derivation outlined below will follow the treatment by Najmabadi et al. (1975). Their derivation is an extension of Lamb's treatment of a two level system to a three level system.

A.1 SEMI-CLASSICAL THEORY OF LASING

Lamb's semi-classical approach to laser theory is one of self-consistency between the lasing media and the electromagnetic field within the laser. The classical electromagnetic field (em) inside the laser resonator interacts with the

excited molecules following quantum mechanic calculations. The sum of these em-molecule interactions, using density matrix methods, gives an expression for the macroscopic polarization of the medium. The complex macroscopic polarization of the medium must obey Maxwell's equation, so that the electric field and thus the intensities of the resonator modes can be calculated. The intensities of the emitted laser radiation are the product of the mode intensities times the transmission of one or the other or both mirrors of the laser resonator.

Usually, the em-molecule interaction is taken to be between the electric field, E, of a plane em wave and the electric dipole of the molecule. The molecule is considered not to have any magnetic sub-levels. Also, the spontaneous decay, the phase loss of the levels from collisions and the excitation of lasing levels are treated phenomenologically for the interaction calculations. A more complete and detailed explanation of the semi-classical theory of lasing can be found in chapter 8 of Sargent et al.(1974), and for multimode lasing in chapter 9 of the same reference.

A.2 THEORY OF COUPLED TRANSITIONS

The different types of coupled transitions were shown in figure 3.1. Because the experiments done for this thesis were done with transitions that were in competition, the following calculation will be done for the competitive case that share an upper level. Only small modification to the signs and

subscripts have to be done for the other competitive case and the cascade case.

For the model, each energy level, i, is pumped at a rate λ_i, has a decay rate of $\delta_i \rho_{ii}$, where δ_i is the decay coefficient and ρ_{ii} is the density matrix population coefficient.

The em field inside the cavity is considered to be a standing wave with the form

$$U_n(z) = \sin(K_n z)$$

where K_n is the wavenumber of the mode n. The frequency of the mode is

$$\omega_n = K_n c = n\pi c/L$$

and where c is the speed of light, n is a large integer (10^6) and L is the cavity length.

The electric field, E, and the corresponding complex polarization of the field , P, can be both represented with a similar type of expansion.

$$E(z,t) = (1/2)\Sigma_n E_n(t)\exp[-i(\omega_n t+\varphi_n)]U_n(z) + cc.$$

$$P(z,t) = (1/2)\Sigma_n P_n(t)\exp[-i(\omega_n t+\varphi_n)]U_n(z) + cc.$$

where both E_n, P_n and φ_n are slowly varying functions of time. ω_n is the frequency of the n'th mode of the resonator. The abbreviation cc. stands for complex conjugate.

As mentioned before, the electromagnetic field inside the cavity must satisfy Maxwell's equation and be self-con

sistent. Following the standard method of Lamb (Scully et al., 1974, Chap 8), The electric field can be related to the polarization inside the cavity by these relations.

$$E_n = -(1/2)[(\nu_n/Q_n)E_n - (\nu_n/\epsilon_o)\mathrm{Im}(P_n), \quad (A.2\text{-}1)$$

$$\nu_n + \varphi_n = \Omega_n - (1/2)(E_n^{-1}\mathrm{Re}(P_n)(\nu_n/\epsilon_o)$$

where Q is the quality factor of the cavity for the mode n (related to the radiation loss of the cavity) and ϵ_o is permittivity of free space.

For a transition i to j, corresponding to a photon of energy $\hbar\nu_j$, the complex polarization can be calculated, using the rotating wave approximation from the integral

$$P_j(t) = 2\exp[i(\nu_j t+\varphi_j)(1/M_j)\int_0^L dz\ U_j^*(z)\wp_{ij}\rho_{ji}(z,t) \quad (A.2\text{-}2)$$

where $\wp_{ij}$ is the dipole moment of the transition, ρ_{ij} is the off-diagonaldenety matrix element ralted to the transition probability, and M_j is the spatial normalization constant evaluated by the integral

$$M_j = \int_0^L |U_j(z)|^2 dz$$

The general equation for the population matrix elements has the form

$$\dot{\rho} = \lambda - (i/\hbar)[H,\rho] - (1/2)(\Gamma\rho+\rho\Gamma),$$

For our case of coupled three level transitions, all the variables and functions of the above equation, are three by three matrices. The operator H is the total Hamiltonian of the system, and $\lambda_{ij} = \lambda_i\delta_{ij}$ and $\Gamma_{ij} = \gamma_i\delta_{ij}$ represent the

excitation and the decay rate of each level, respectively.

The coupled equation of motion of the population matrix element are as follows.

$$\dot{\rho}_{32} = -(i\omega_{32}+\gamma_{32})\rho_{32} + (i/\hbar)\upsilon_{32}(\rho_{33}-\rho_{22}) + (i/\hbar)\upsilon_{12}\rho_{31}$$

$$\dot{\rho}_{21} = -(i\omega_{21}+\gamma_{21})\rho_{21} + (i/\hbar)\upsilon_{21}(\rho_{22}-\rho_{11}) + (i/\hbar)\upsilon_{23}\rho_{31}$$

$$\dot{\rho}_{31} = -(i\omega_{31}+\gamma_{31})\rho - (i/\hbar)(\upsilon_{32}\rho_{21} - \rho_{32}\upsilon_{21})$$

$$\dot{\rho}_{33} = \lambda_3 - \gamma_3\rho_{33} + [(i/\hbar)(\upsilon_{32}\rho_{23} + cc.)]$$

$$\dot{\rho}_{22} = \lambda_2 - \gamma_2\rho_{22} + [(i/\hbar)(\upsilon_{32}\rho_{23} + cc.)] - [(i/\hbar)(\upsilon_{21}\rho_{12} + cc.)]$$

$$\dot{\rho}_{11} = \lambda_1 - \gamma_1\rho_{11} + [(i/\hbar)(\upsilon_{21}\rho_{12} + cc.)]$$

$$\gamma_{ij} = (1/2)(\gamma_i+\gamma_j) + \gamma_{ij}^{phase}$$

and γ_{ij}^{phase} coefficient is included to account for the dephasing between the two levels by molecular collisions. The υ_{ij} term represent the interaction energy of the electric field with the electric dipole of the molecule.

$$\upsilon_{ij} = -E(z,t)\mu_{ij}$$

where μ_{ij} is the electric-dipole element between the two lasing levels. Using the rotating wave approximation, υ_{ij} has the form

$$\upsilon_{ij} = -(1/2)\mu_{ij}E_j(t)\exp[-i(\nu_j t+\phi_j)]U_j(z)$$

The variables ρ_{11}, ρ_{22}, ρ_{33}, ρ_{12}, ρ_{23}, ρ_{31} can be evaluated using third order perturbation methods. The values of ρ_{12} and ρ_{23} can be used for the evaluation of P_1 and P_2

from the integral (equation A.2-2). The values of P_1 and P_2 can then be used to evaluate the electric field strength and the frequency inside the cavity (equation A.2-1). The electric field of each mode then has the form

$$\dot{E}_1 = E_1(\alpha_1 - \beta_1 E_1^2 - \theta_{12} E_2^2) \quad \text{(A.2-3a)}$$

$$\dot{E}_2 = E_2(\alpha_2 - \beta_2 E_2^2 - \theta_{21} E_1^2) \quad \text{(A.2-3b)}$$

where α_1, α_2 are the net gains of the laser for the transition 1 and 2, β_1, β_2 are the the saturation parameters of the transition 1 and 2, and θ_{12}, θ_{21} are the cross saturation terms that couple the the intensity of transition 2 to transition 1, and 1 to 2, respectively. The frequency of each mode has the form

$$\nu_1 + \dot{\phi}_1 = \Omega_1 + \sigma_1 - \rho_1 E_1^2 - \tau_{12} E_2^2 \quad \text{(A.2-4a)}$$

$$\nu_2 + \dot{\phi}_2 = \Omega_2 + \sigma_2 - \rho_2 E_2^2 - \tau_{21} E_1^2 \quad \text{(A.2-4b)}$$

where σ_1, σ_2 are the linear mode pulling terms and ρ_1, ρ_2 are the mode pushing terms of transition 1 and 2, while τ_{12}, τ_{21} are the cross pushing term that couples the frequency of transition 2 to transition 1, and 1 to 2, respectevely. The explicit forms of α_1, α_2, β_1, β_2, θ_{12}, θ_{21}, σ_1, σ_2, Ω_1, Ω_2, τ_{12}, τ_{21} involving electric dipole matrix coefficient, population inversion, frequency offset of resonator modes from the transition line center, decay rates of laser levels, Q's of resonator modes and frequencies of the laser transitions for homogeneous broadened competitive line can be found in the following table. A more complete list for all the combinations of lines in cascade or competition, inhomogeneously or homogeneously broadened can be found in Najma-

badi et al. (1975).

w_{23}	frequency of the transition level 2 to 3
ν_2	mode frequency for the transition 2-3
ν_1	mode frequency for the transition 2-1
$N_{i,i-1} = \rho_{ii}^{(0)} - \rho_{i-1,i-1}^{(0)}$	unsaturated population difference
$\bar{N}_{i,i-1} = (1/L) \int_0^L N_{i,i-1}(z,t)dz$	average population difference
$\mathcal{L}_x(\Delta w) = \gamma_x^2/[\gamma_x^2 + (\Delta w)^2]$	Lorentzian function
$D_x(\Delta w) = 1/[\gamma_x + i(\Delta w)]$	complex denominator
$\alpha_2 = -(\nu_2/2Q_2) + F_{32}^{(1)} \mathcal{L}_{32}(w_{32}-\nu_2)$	linear net gain
$\beta_2 = \mathcal{L}_{32}^2(w_{32}-\nu_2)F_{32}^{(3)}$	self-saturation
$F_{32}^{(1)} = (1/2)(\mathcal{P}_{32}^2/\hbar\epsilon_0\gamma_{32})N_{32}$	first order factor
$F_{32}^{(3)} = (3/2)(\mathcal{P}_{32}/2\hbar)^2(1/\gamma_{32})F_{32}^{(1)}(1/\gamma_3 + 1/\gamma_2)$	third order factor
$\sigma_2 = (1/\gamma_{32})(w_{32}-\nu_2)\mathcal{L}_{32}(w_{32}-\nu_2)F_{32}^{(1)}$	linear mode pulling
$\rho_2 = (1/\gamma_{32})(w_{32}-\nu_2)\mathcal{L}_{32}^2(w_{32}-\nu_2)F_{32}^{(3)}$	self-pushing
$\tau_{nm} + i\theta_{nm} = \vartheta_{nnmm} + \vartheta_{nmnm}$	cross-saturation terms
$\vartheta_{2211} = (1/8)i\nu_2[(\mathcal{P}_{32}\mathcal{P}_{31})^2\bar{N}_{21}/\hbar^3\epsilon_0\gamma_3\gamma_{31})] \times D_{32}(w_{32}-\nu_2)\mathcal{L}_{31}(w_{31}-\nu_1)$	complex cross-saturation population depletion part
$\vartheta_{2121} = (1/8)iF_{32}^{(1)}\gamma_{32}(\mathcal{P}_{31}/\hbar)^2 D_{32}(w_{32}-\nu_2)D_{21}(\nu_1-\nu_2-w_{21}) \times [(\bar{N}_{31}/\bar{N}_{32})D_{31}(\nu_1-w_{31}) + D_{32}(w_{32}-\nu_2)]$	complex cross-saturation electric-quadrupole part

Table A.1
Summary of coefficient for competitive coupled transitions
Equations are for transitions 32 (bc in figure 3.1), for 21 transitons, same as above but with the substitutions 2<-->1, 32<-->12, and γ_3<-->γ_1

APPENDIX B

METAL EVAPORATION TECHNIQUES FOR MIRROR FABRICATION

This appendix describes the fabrication technique of a front surface mirror by the evaporation deposition method of gold or aluminum. Most of the information in this appendix has been gained from experience. However, the technique of coating silicon was obtained from Brian Roberts, head of Production in the Optics Division of the National Research Council of Canada (private communication). All the mirrors used for the experiments including the lasers principal mirror were coated in our evaporator with gold over nickel.

B.1 ALUMINUM COATING

As a rule, coating any surface with aluminum is easy. For best results, the surface should be chemically cleaned, rinsed and left without any residual streaks. To remove a previous aluminum coating, a warm 0.5 molar solution of potassium hydroxide (KOH) (12 grams of KOH with 500 milliliters of warm water) should remove it quickly. If the aluminum surface to be removed has protective silicon monoxide (SiO) overcoat, place the mirror in a 1.0 molar KOH solution. To accelerate the removal process, place the

solution vessel in an ultrasonic bath for several hours. The coating will slowly dissolve uniformly across the surface in about 12 hours.

For a typical distance between the evaporation boat and the substrate of 85 millimeters (that found in the laboratory system, Edwards Vacuum Coating Unit, model E12E3), about 20 milligrams of pure aluminum should be evaporated to make a totally reflecting mirror. The aluminum will melt and evaporate when the molybdenum boat is cherry red (melting point of aluminum is 660 degrees Celsius).

The thickness of the metal coating scales linearly with the amount of metal evaporated, and inversely to the square of substrate to boat distance. From these relations, the amount of metal can be adjusted for different evaporation distances.

B.2 GOLD COATING

To coat any surface like glass or silicon with gold is much more difficult than with aluminum. Unless properly done, the gold coating will not adhere to the substrate properly, and the gold will flake off.

To make gold mirrors, the surface must be first cleaned chemically and rinsed as best as possible: the 0.5 molar KOH solution, described in the previous section, is a good

cleaning agent. The procedure described in the previous section to remove SiO overcoat surface will also remove an old gold coating. The KOH solution will not dissolve the gold, but the procedure will promote the gold to separate from the substrate. Wiping the surface with a camel hair artist paint brush while the substrate is in the solution will also help remove the coating. If needed, the gold surface can be dissolved with aqua regia (a mixture of hydrochloric and nitric acids, also good for dissolving platinum).

The following procedure is for the deposition of gold on a silicon or glass substrate to make a partially reflecting mirror. (A simpler procedure is described below for making totally reflecting gold mirrors.) The substrate is placed in the evaporator and under vacuum, and further cleaned with an RF discharge (usually with argon) for 5 to 10 minutes. Before depositing the gold, the substrate should be heated between 100 and 200 degrees Celsius. The gold should be evaporated quickly on to the substrate from a white hot molybdenum boat (gold's melting temperature is 1063 degrees Celsius). Once the substrate is coated, it should be further baked at 250 degrees Celsius for 30 minutes, or alternatively, the surface should be irradiated with a carbon dioxide laser for a similar period.

The transmission of a semi-transparent gold mirror

depends on the amount of gold deposited, the wavelength of the radiation and on transmission properties of the substrate. Some experimentation and calibration must be done for a specific application. For example, it has been found experimentally that a glass cover slide (#1 thickness) will have 36 percent transmission for 3.39 micrometer radiation when coated with 2.8 milligrams of gold at 85 millimeters substrate to boat distance. The uncoated glass has 89 percent transmission for 3.39 micrometer radiation (C.W. Schneider, private communication).

To make totally reflecting gold mirrors, the gold coating can be deposited on a clean surface of nickel, Inconel or chromium: only gold on nickel mirror have been fabricated in our laboratory. This procedure does not need any special cleaning or heating process, the surface only needs to be chemically cleaned, rinsed and left without any residual streaks. Because nickel forms an alloy with molybdenum, a tungsten coil must be used to evaporate the nickel (65 milligrams of nickel at 85 millimeters coil to substrate distance). The tungsten coil must be white hot because the melting temperature of nickel is 1455 degrees Celsius. It also appears that the tungsten coil forms an alloy with the nickel at these high temperatures because the coils can only be used for 3 or 4 coatings before breaking[1]. Without

[1] There are evaporation boats available that are coated with an aluminum oxide surface that are not attacked by the molten nickel.

breaking the vacuum, the gold is then deposited upon the fresh nickel surface (60 milligrams of gold at 85 millimeters boat to substrate distance). The resulting mirror can still be scratched easily but, with a delicate touch and care, can be wiped or cleaned.

REFERENCES

G.S. Agarwal and S. Dattagupta, "Higher-order phase transitions in systems far from equilibrium: Multicritical points in two-mode lasers", Physical Review A, 26, 880 (1982).

J.P. Auton, "Infrared Transmission Polarizers by Photolithography", Applied Optics, 6, 1023 (1967).

G.P. Agrawal, "Atomic coherence effects in a two-mode laser with coupled transitions", Physical Review, 30, 884 (1984)

W.S. Benedict, M.A. Pollack and W.J. Tomlinson, III, "The Water-Vapor Laser", IEEE Journal of Quantum Electronics, QE-5, 108 (1969).

I.M. Beterov and V.P. Chebotaev, "Three-level gas systems and ther interaction with radiation", Progress in Quantum Electronics, 3, pt.1 (1974).

E. Brannen, "Reflection Gratings as Elements in Far Infrared Masers", Proc. IEEE, 53, 2134 (1965).

E. Brannen and D. G. Rumbold, "Reflectivity and Polarization Characteristics of Reflection Echelette Gratings", Applied Optics, 8, 1506 (1969).

E. Brannen and W.J. Sarjeant, "Far-Infrared Laser Action Using Compound Grating Frabry-Perot Resonators", IEEE Journal of Quantum Electronics, QI-5, 138 (1970).

F.C. Choo and E. Brannen, "Grating Coupled Compound Resonators". Applied Optics, 10, 1919 (1971).

R.C. Compton, L.B. Whitbourn and R.C. McPhedran, "Simple Formulae for the transmittance of strip gratings", Journal Infrared and Millimeter Waves, 4, 901 (1983).

E.U. Condon and Shortley, The theory of atomic spectra, Cambridge University Press, London (1935).

H. Haken, R. Der Agobian and M. Pauthier, "Theory of Laser Cascades", Physical Review, 140, A437 (1965).

F.T. Hioe and S. Singh, "Correlations, transients, bistability, and phase transition analogy in two-mode lasers", Physical Rewiew A, 24, 2050 (1981).

M. Hoeksema, W.J. Sarjeant and E. Brannen, "Far-Infrared Gas Laser as Sources of Linearly Polarized Radiation", IEEE Journal of Quantum Electronics, QE-5, 478 (1969).

I.H. Hutchinson, "Polarization modulation of a submillimetre laser". Optics Communications, 38, 201 (1981).

I.H. Hutchinson, "The phase of reflection from a conducting grating". Optics Communications, 39, 1 (1981).

I.H. Hutchinson, "A heterodyne plasma interferometer base on polarisation modulation of a HCN laser". Journal of Physics E: Scientific Instrumentation, 15, 343 (1982).

M.C. Hutley, Diffraction gratings (Techniques of physics) Academic Press Inc. (London) Ltd., London (1982).

W.Q. Jeffers, "An experimental test of proposed water-vapor laser transition assignments", Applied Physics Letters, 13, 104 (1968).

M.F. Kimmitt, Far-Infrared techniques, Pion Ltd., London (1970).

L.M Khayutin, "Lasers based on couple transitions with arbitrary polarization of radiation", Optical Spectroscopy (USSR), 47, 527 (1979).

L.M Khayutin, "Polarization effects in the interaction between waves generated by coupled-transition lasers", Optical Spectroscopy (USSR), 49, 194 (1980).

D.A. Kleinman and P.P. Kisliuk, "Discrimination Against Unwanted Orders in the Fabry-Perot Resonatror", Bell System Technical Journal, 41, 453 (1962).

G.V. Melekhin and G.P. Melekhina, "Effect of radiation polarization on the interaction of modes of two lasing channels by a common level", Optical Spectroscopy, 35, 420 (1974).

F. Najmabadi, M. Sargent III and F. A. Hopf, "Theory of laser oscillation on two or more coupled transitions", Physical Review A, 12, 1553 (1975).

A.H. Paxton an P.W. Milonni, "Semiclassical Theory of Three-level gas lasers", Optics Communicatios, 34, 111 (1980).

R. Petit, Electromagnetic theory of gratings (Topics in current physics), Springer-Verlag, Berlin (1980).

E.H Putley, Optical and Infrared Detectors, Ed: R.T. Kayes, chapter 3, p. 71, Springer Verlag, Berlin (1980).

P.A. Rochefort, "A Study of a CW and Pulsed Infrared Water Vapour Laser", M.Sc. Thesis, The University of Western Ontario (1981).

M. Sargent III, M.O. Scully, W.E. Lamb, Jr., Laser Physics, Addison-Wesley, Reading, Mass. (1974).

W.J. Sarjeant and E. Brannen. "A current transformer for microsecond pulses", Proc. IEEE, 56, 359 (1968).

W.J. Sarjeant and E. Brannen. "Comment on a current transformer fo microsecond pulses", Proc. IEEE, 56, 1594 (1968).

S. Singh and M.S. Zubairy, "Quantum theory of a two-mode laser with coupled transitions", Physical Review A, 21, 281 (1980).

S. Singh and M.S. Zubairy, "Intensity correlations in a two-mode laser with coupled transitions", Physical Review A, 23, 2507 (1981).

I.I. Sobel'man, Introduction to the theory of atomic spectra, Pergamon Press, Oxford (1972).

D. Véron and L.B. Whitbourn. "Strip gratings on Dielectric substrates as output coupleŗs for submillimeter lasers", Applied Optics, 25, 619 (1986).

L.B. Whitbourn, J.C. Macfarlane, I.S. Falconer, B.W. James and P.A. Stimson, "Polarization switching in a strip grating coupled optically pumped submillimete laser", yApplied Physics Letters, 48, 957 (1986).

coupling when the two lines were parallel to each other, opposite to what was expected from the given energy level assignments. For the 26.6-47.47 micrometer, the 27.97-47.70 micrometer and the 27.97-47.47 micrometer interaction experiments, the power of the short wavelengths did not change noticeably with the experimental noise level to be able to calculate coupling constants.

Several polarization reflection properties of the primary grating for radiation of wavelengths longer than the critical wavelength were investigated by using the MGG laser in single mode configuration and lasing from the secondary grating. The reflection coefficient of the primary grating for radiation polarized parallel to the grating lines was found to be greater than for perpendicularly polarized radiation. This is an important feature for the design of a MGG laser when maximum power of two non-interacting lines is wanted.

The polarization of the second line in the MGG compound resonator was found to be parallel or perpendicular (or both in a special case) to the primary grating lines as the secondary grating was rotated about the optical axis. This feature is consistent with the grating model of a difference in position of optical plane of reflection for parallel and perpendicular polarized radiation.